Kinetics of metal detection by luminescence-based whole-cell biosensors: connecting biosensor response to metal bioavailability, speciation and cell metabolism

Jérôme Duval, Lorenzo Maffei, Eva Delatour, Marie Zaffino, Christophe Pagnout

Kinetics of metal detection by luminescence-based whole-cell biosensors: connecting biosensor response to metal bioavailability, speciation and cell metabolism

Jérôme F.L. Duval,[1,*] Lorenzo Maffei,[2] Eva Delatour,[2] Marie Zaffino,[2] Christophe Pagnout[2]

[1] Université de Lorraine, CNRS, LIEC, F-54000 Nancy, France.
[2] Université de Lorraine, CNRS, LIEC, F-57000 Metz, France.
* Corresponding author (jerome.duval@univ-lorraine.fr).

GRAPHICAL ABSTRACT.

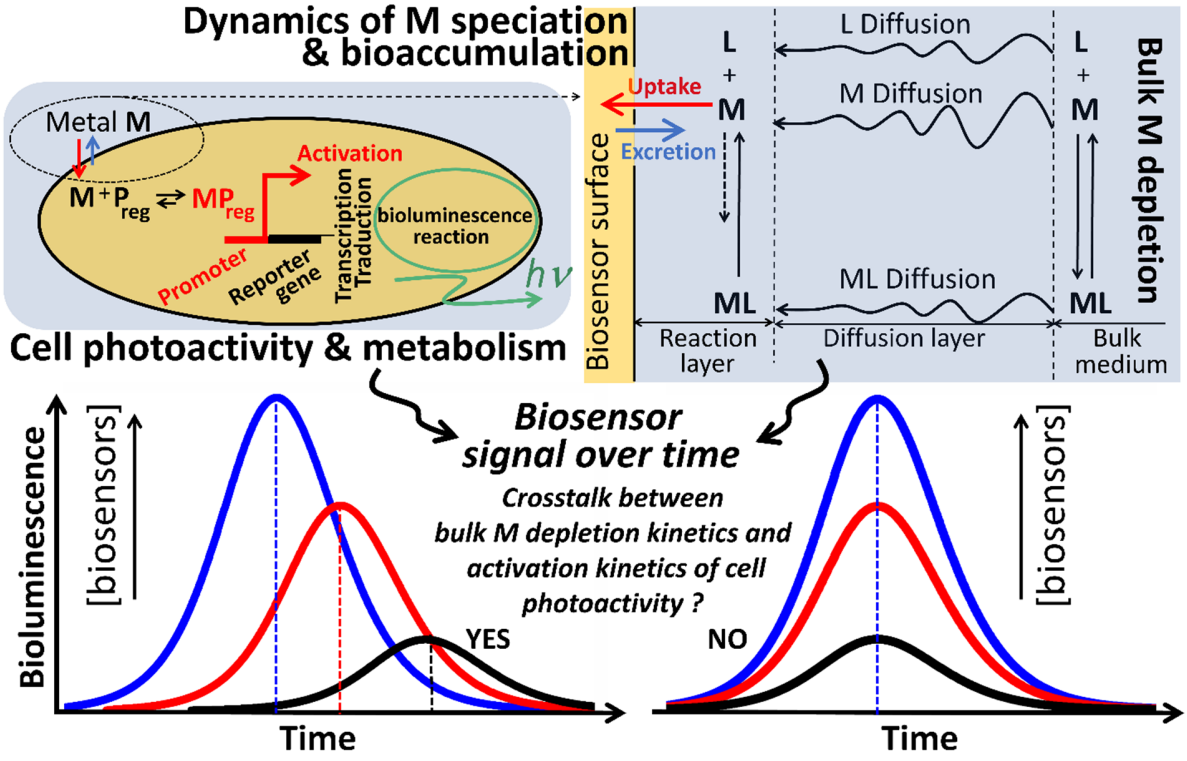

Keywords. Bioluminescence, Whole-cell metal bioreporters, Metal bioavailability, Metal speciation, Biointerfacial metal partitioning, Biophysicochemical theory.

Abstract.

Luminescent whole-cell metal biosensors are genetically engineered cells used for the detection of metals in e.g. aqueous solutions. Herein, we detail the quantitative connections between time-response of luminescent bacterial metal sensors and the bioavailability of free and complexed metal species. To that end, we formulate the biophysicochemical dynamics of metal partitioning at a biosensor/solution interface and integrate the required metabolism contribution to cell response. The formalism explains the ways in which cell signal depends on: coupled Eigen kinetics of metal complexation and diffusion of metal species to/from the interface; kinetics of metal excretion, Michaelis-Menten bioaccumulation and ensuing metal depletion from bulk solution; and kinetics of bioluminescence production following intracellular metal sequestration by regulatory metalloproteins. In turn, an expression is derived for the time-dependent cell signal as a function of interrelated (bioavai)lability of metal species and (thermo)dynamic descriptors of extra/intracellular metal complexation. Quantitative criteria are elaborated to identify scenarios where equilibrium modeling of metal speciation is incorrect, bulk metal depletion is operative, metal biouptake kinetics is governed by metal diffusion, or labile metal complexes fully contribute to cell response. Remarkably, in agreement with experiments, the theory predicts time-shifts of bioluminescence peaks with increasing concentration of biosensor and/or metal ligand in solution. We show that these shifts originate from the crosstalk between activation kinetics of cell photoactivity and speciation-dependent kinetics of bulk metal depletion. Overall, the work paves the way for the elaboration of new strategies to exploit the bioluminescence response of metal *lux*-biosensors at a dynamic level and evaluate metal bioavailability properties in environmental or biological aqueous samples.

1. Introduction.

Persistence, bioaccumulation potential and toxicity are key factors currently used to classify metals (**M**) that pose a risk to living organisms in aqueous environmental media. Due to their interactions with organic and inorganic metal-binding ligands (**L**), metals exist in various physicochemical forms or species (**ML**) that differ in terms of chemical reactivity, which in turn impacts on their fate, transport, bioavailability and toxicity.[1] Accordingly, metal risk assessment generally requires the evaluation of metal speciation in solution.[2] This explains why much effort has been spent on developing equilibrium models that predict the solubility and stability of complexed metal forms, e.g. NICA-Donnan, WHAM and extensions thereof, and freeware chemical models like Visual MINTEQ.[3-6] The relationship between metal speciation and bioavailability to metal-accumulating microorganisms (e.g. bacteria, microalgae) has further received a lot of attention in literature.[1] In particular, the Biotic Ligand Model (BLM) makes the distinction between total metal activity and activity of free (not complexed) metal M as the determinant bioavailability parameter.[7] In detail, BLM assumes a priori the existence of a full equilibrium between M activities in bulk solution and at the surface of the metal-consuming microorganism, so that the only parameter controlling metal bioavailability of bioinactive (i.e. non-bioaccumulated) ML complex is the bulk activity of M.[8,9] Within such an equilibrium representation of metal species partitioning at microorganism/medium interfaces, metal complexation therefore leads only to a decrease in the bulk concentration of free metal ions M.

Whereas BLM constitutes an interface within regulatory arena, its failure to predict metal bioaccumulation has long been reported for a variety of organisms and metals under both complexing *and* non-complexing medium conditions.[8-12] One of the BLM limits at the origin of such a failure stems from its restrictive equilibrium-based assessment of the dynamic processes that control the intertwined reactive transport of metals (free and complexed) from the solution to the microorganism and the accumulation of the bioactive free metal forms (or any others if relevant).[8-12] In particular, BLM does not account for the lability of metal complexes, i.e. the extent to which ML dissociates and releases free M on the timescale of its diffusion towards the bioaccumulating surface.[11-14] Then, depending on the demands of the organism and on the lability of ML complex, the latter may dissociate in the vicinity of the organism and thereby *contributes* to the biouptake of free M (**Figure 1**).[11,13,14] Concepts have been developed for describing the dynamics of chemical speciation in aqueous media in the context of an ongoing interfacial process that consumes free metals at a given surface, may it be a metal-sensor or a microorganism.[9] Based on these concepts, it was shown that applicability of BLM is conditioned to a sufficiently fast transport of metal species in solution as compared to the actual metal uptake so that the latter is rate-determining.

An additional limitation in the application of BLM when combined to classical thermodynamic speciation computations is its incapacity to address whether or not metal depletion from bulk solution is operative during bioaccumulation.[12,15-17] This issue is however crucial as metal depletion - when significant - leads necessarily to a decrease in bioavailable M concentration over time. Theoretical studies confronted to experiments have solved this problem on the basis of a *non-equilibrium flux-based approach* with or without account of metal speciation in solution, intracellular M complexation and organism ability to excrete internalized M for detoxification purpose.[12,15-19] The common denominator of these studies is their modelling of M biointerfacial partitioning without invoking a priori the equilibrium hypothesis formulated in BLM.

Parallel to the above modelling developments on metal bioavailability, the advent of cutting-edge biotechnologies like luminescent whole-cell metal bacterial reporters (or biosensors) has provided environmental chemists with a tool to *measure* bioavailable metal concentration in aqueous solution (**Figure 1**).[20] Briefly, *lux*-reporter genes introduced in a given host bacterium are fused to a promoter whose expression is regulated by a regulatory (or repressor) protein, P_{reg}, that has a strong affinity for the metal to be detected. In the absence of the metal, the expression of the reporter gene is repressed by the repressor attached to the promoter and bacteria do not produce luminescence. Inactivation of the repressor occurs when the latter forms a MP_{reg} complex with internalized M, which initiates the expression of *lux* gene and the production of the reactants required for bioluminescence reaction, including the reporter protein (luciferase) that acts as a reaction catalyst.[20] Advantages of so-engineered metal biosensors include the possible exploration of a large spectrum of metal speciation scenarios *via* cost-effective *and* automated measurement of the bioluminescence response over several tens of hours with minute-timestep resolution.[21] However, despite the (apparent) simplicity of their functioning, one of the clear downsides to the use of metal *lux*-bioreporters is that interpretation of the bioluminescence signal is far from easy. Indeed, quantifying metal bioavailability from bioluminescence output requires not only the integration of the relevant physical and chemical processes that determine biointerfacial metal partitioning over time (**Figure 1**),[22] but also the way in which cell metabolism of nutrients from the medium can sustain light production after metal-triggered actuation of the promoter.[21,23] As an illustration, recent work demonstrated that cell stringent response and catabolite repression may lead to bioluminescence signals over time that feature one, two or three peaks depending on the bioavailability of amino acids and sugars in solution, some of these peaks being doublets or even presenting marked truncations.[21,23] Due to this complexity, the exploitation of bioluminescence cell signals remains essentially limited so far to (i) mere consideration of the only maximal signal amplitude without

114 mechanistic analysis of the signal dependence on time, (ii) the recourse to calibration measurements for
115 converting bioluminescence into bulk concentration of free metal estimated by thermodynamic
116 speciation computations within restrictive equilibrium BLM framework, or (iii) empirical fitting of time-
117 dependent bioluminescence data collected for different metal contents in solution.[20,24-26]

118 In view of the above elements, force is to recognize the lack of a comprehensive theory for a full
119 exploitation of the time-response of luminescent metal biosensors and the evaluation of metal
120 bioavailability properties beyond the limits of equilibrium BLM. Accordingly, we extend herein our recent
121 model on bioluminescence emission by metal biosensors[22] to cases where media contain metal-binding
122 ligands *and* metal may be depleted from bulk solution in the course of time. Following the idea in [22],
123 the model integrates the contribution of cell metabolism to the produced signal via a differentiation
124 between photoactive and photoinactive cells in solution. It further formulates explicitly the connection
125 between bioluminescence signal and bioavailability of metal species, which includes not only bioactive M
126 but also labile ML that can contribute to M biouptake flux. The analysis accounts for cell metal excretion,
127 metal complexation by intracellular repressor protein, interconversion between M and ML forms during
128 their (coupled) diffusions to the biosensor surface, and depletion of M from bulk solution as a result of M
129 bioaccumulation by the metal-sensing cells. Among the important results reported here, we demonstrate
130 how *the amplitude*, *shape and time of apparition* of the bioluminescence signal depend on the
131 concentrations of biosensor and metal-binding ligand in solution, and how these signal properties reflect
132 the thermodynamic *and* kinetic determinants of metal speciation and related metal bioavailability
133 features. Accordingly, this work defines a solid theoretical basis for the development of new procedures
134 to unravel the contributions of biology (cell metabolism) and interfacial physical-chemistry (metal
135 bioavailability/speciation) to the bioluminescence response of metal *lux*-biosensors.
136
137
138

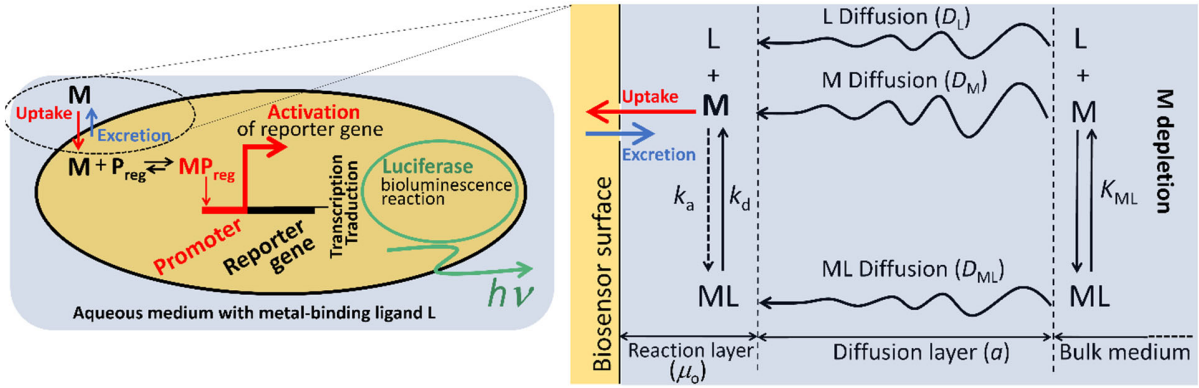

Figure 1. (Left panel) Simplified scheme for the functioning principle of a metal (M)-responsive luminescent bacterial sensor. **(Right panel)** Schematics of the transport and chemical kinetic contributions to the overall flux of (bioactive) metal ions at the interface between a metal biosensor and aqueous solution. The work aims at formulating quantitatively the connections between the time-dependent bioluminescence response of the biosensor, and the bioavailability of the metal species via account of the interplay between metal complex (ML) chemodynamics, diffusive transports of M, metal-binding ligand (L) and ML (with associated diffusion coefficients $D_{i=\mathrm{M,L,ML}}$), and kinetics of metal depletion from bulk solution. In the right panel, the reaction layer (thickness μ_o) and the diffusion layer (thickness *a*, the curvature radius of the metal-sensing bioparticle) are indicated. See text for details.

2. Dynamics of biointerfacial metal partitioning: governing equations, results and discussion.

2.1. Setting the stage.

We consider an aqueous medium of volume V_T containing metal-accumulating bacteria (the bioluminescent metal biosensors) assimilated to spheres of radius a, metal ions M and metal-binding ligands L (**Figure 1**). The complexation reaction M+L↔ML leads to the formation of ML complexes with stability constant denoted as K_{ML} ($m^3\ mol^{-1}$) defined by $K_{ML} = k_a / k_d$ where k_a ($m^3\ mol^{-1}\ s^{-1}$) and k_d (s^{-1}) are the kinetic constants for ML formation and dissociation, respectively. Expressions of k_a and K_{ML} for the here-considered molecular ligands L follows Eigen mechanism for ions pair association[27] and Eigen-Fuoss theory,[28,29] respectively. The total concentration of bacteria is expressed by their number density c_B (in m^{-3}) taken independent of time t for the sake of simplicity. The formalism is thus applicable to situations where bacterial growth is insignificant, which is achieved in minimal nutritive media.[21-23] c_B is related to the volume fraction of bacteria in solution φ via $c_B = \varphi / V_B$ with $V_B = 4\pi a^3 / 3$ the volume of an individual bacterium. The developments below hold under conditions where the electrostatic charges distributed at the surface of the metal-sensing cells are screened, i.e. in media whose ionic strength is sufficiently high. At $t = 0$, metal ions are introduced in the medium with bulk concentration $c_M^{*,0}$ ($mol\ m^{-3}$). For the sake of demonstration, free metal ions M are viewed as the only metal species that can be accumulated by the bacteria (i.e. they are the only bioactive metal forms) and excreted to some extent

via dedicated metal efflux pumps. We denote as k_e (s^{-1}) the kinetic constant for metal excretion, and the corresponding metal excretion flux, J_e (mol m^{-2} s^{-1}), is written $J_e = k_e \phi_M$ where ϕ_M (mol m^{-2}) is the concentration of intracellular free M expressed per microorganism surface area.[12,30-32] After their internalisation, free metal ions are bound by the intracellular regulatory proteins P_{reg} to form metal complexes, MP_{reg}. In the following, we denote as $k_{a,i}^*$ and $k_{d,i}^*$ the kinetic constants of association between M and P_{reg}, and dissociation of intracellular MP_{reg}, respectively. Based on theory for chemodynamics of complexes formed between metals and nanoparticulate ligands (P_{reg} being a representative thereof),[33-35] the constants $k_{a,i}^*$ and $k_{d,i}^*$ integrate here the coupling between the conductive-diffusion transport of intracellular free M to/from the metal binding sites carried by P_{reg} and the kinetics of the chemical binding step. The MP_{reg} complexes interact with the promoter placed upstream the *lux* reporter gene (**Figure 1**), which initiates the transcription of that gene and the production of the reporter protein (luciferase) that plays a central role in bioluminescence reaction. The modelling of the kinetics of the intracellular biochemical reactions leading to bioluminescence, from the very activation of the promotor by MP_{reg} to the production of luciferase, follows the scheme we formulated elsewhere[22] for metal biosensors under non-complexing medium conditions in the absence of metal depletion from bulk solution.

Following previous reports,[12,17] it is convenient to formulate the spatial distribution of biosensors in solution according to a Kuwabara cell representation. Within the framework of the latter, each individual metal-sensing bacterium is enveloped by a virtual cell of radius r_c such that the bacterium/solution volumes ratio in that cell equates with the one prevailing in the entire medium, i.e. $r_c = a\varphi^{-1/3}$. Due to the accumulation of M in the bacterial body (internalisation), the concentration of M in bulk solution at time *t*, denoted as $c_M^*(t)$ (mol m^{-3}), may differ from $c_M^{*,0}$ as a result of M depletion from bulk solution. Steady-state M diffusion is readily achieved at any *t* for organisms with micrometric dimension like bacteria,[15] and the corresponding ~ms timescale required for building up a metal diffusion layer at the organism/solution interface (transitory diffusion regime) is much faster than the typical timescales associated with M internalisation and depletion from bulk solution (~mins to hrs).[15,16,18] It was further shown[15] that *steady-state* M transport from solution to the M-accumulating biosurface actually applies at any *t* while M bulk concentration is being depleted provided that φ is much lower than unity (in line with typical bioassays conditions). The radial coordinate *r* is adopted and the origin is taken at the microorganism centre. The position $r = a$ marks the location of the membrane where M internalisation takes place via dedicated metal transporters. A glossary of all symbols adopted in this work is provided at the end of the document to facilitate reading. We specify that possible medium- and metal-induced

toxicity effects on cells are not considered here, meaning that (photoactive and photoinactive) bacteria are alive during the entire duration of bioluminescence assays. This situation corresponds to experimental conditions commonly adopted in practice to monitor bioavailability of trace metal ions with metal-sensing bacteria.

In the developments below, we determine the spatial distributions of M, L and ML over time in the extracellular domain $\left(a \le r \le r_{\mathrm{c}}\right)$ and the expression of the metal bioaccumulation flux as a function of the relevant thermodynamic and kinetic descriptors of the problem (§2.2). We then formulate the connection between metal bioavailability properties and bioluminescence response of the metal-sensing bacteria (§3.1), and we discuss the outcome of theoretical predictions with few computational examples that illustrate the dependence of signal amplitude, shape and apparition delay on the concentrations of biosensor and metal-binding ligand in solution (§3.2-§3.3). The expressions reported hereafter for the time-response of luminescent metal biosensors and for metal partitioning at the biosensor/medium interface under bulk metal depletion condition were derived with the support of PTC Mathcad Prime 8 calculus environment. All demonstrations are available upon request, together with the numerical code developed to simulate biosensor signals.

2.2. Metal bioavailability at the biosensor/solution interface under bulk metal depletion condition.

2.2.1. Extracellular distribution of metal species, expression of metal supply flux at the biosensor surface.

Under the conditions detailed in §2.1, the concentration profiles of M, L and ML in the diffusion layer are at steady state while free metal M is being depleted in bulk solution on a time scale much longer than the time needed for the re-adjustment of the M concentration profile.[15] In turn, the spatial distributions of M, L and ML concentrations over time, $c_{i=\mathrm{M,L,ML}}\left(r,t\right)$, are governed by the coupled steady-state Nernst-Planck equations corrected for the kinetic terms pertaining to chemical ML formation and dissociation

$$\begin{cases} D_{\mathrm{M}}\nabla_r^2 c_{\mathrm{M}}\left(r,t\right) + k_{\mathrm{d}}c_{\mathrm{ML}}\left(r,t\right) - k_{\mathrm{a}}c_{\mathrm{ML}}\left(r,t\right)c_{\mathrm{L}}\left(r,t\right) = 0 & \text{(a)} \\ D_{\mathrm{ML}}\nabla_r^2 c_{\mathrm{ML}}\left(r,t\right) - k_{\mathrm{d}}c_{\mathrm{ML}}\left(r,t\right) + k_{\mathrm{a}}c_{\mathrm{ML}}\left(r,t\right)c_{\mathrm{L}}\left(r,t\right) = 0 & \text{(b)} \\ D_{\mathrm{L}}\nabla_r^2 c_{\mathrm{L}}\left(r,t\right) + k_{\mathrm{d}}c_{\mathrm{ML}}\left(r,t\right) - k_{\mathrm{a}}c_{\mathrm{M}}\left(r,t\right)c_{\mathrm{L}}\left(r,t\right) = 0 & \text{(c)} \end{cases} \quad (1)$$

where ∇_r^2 is the Laplacian operator in spherical geometry. For cases of practical interest, L is in large excess over M so that L concentration is essentially independent of r and *t*, and Eq. (1c) reduces to $c_{\mathrm{L}}\left(r,t\right) = c_{\mathrm{L}}^*$ where c_{L}^* is the bulk concentration of L.[36] In bulk solution, *far* from the surface of the microorganisms, equilibrated M and ML concentrations are related linearly by $\overline{K}_{\mathrm{ML}} = c_{\mathrm{ML}}^*\left(t\right) / c_{\mathrm{M}}^*\left(t\right)$ where

$c^{*}_{i=\mathrm{M,ML}}(t)$ are the bulk concentrations of M and ML at *t*, and $\overline{K}_{\mathrm{ML}}$ is the dimensionless ML stability constant defined by $\overline{K}_{\mathrm{ML}} = K_{\mathrm{ML}} c^{*}_{\mathrm{L}}$. The boundaries associated with the coupled differential Eqs. (1a)-(1b) are provided by

$$\begin{cases} c_{i=\mathrm{M,ML}}(r = r_{\mathrm{c}}, t) = c^{*}_{i=\mathrm{M,ML}}(t) & \text{(a)} \\ c_{\mathrm{M}}(r = a, t) = c^{\mathrm{a}}_{\mathrm{M}}(t) & \text{(b)} \\ D_{\mathrm{ML}}\left(\partial c_{\mathrm{ML}}(r,t) / \partial r\big|_{r=a}\right) = 0 & \text{(c)} \end{cases} \tag{2}$$

where Eq. (2a) reflects bulk condition, Eq. (2b) specifies that M concentration identifies with $c^{\mathrm{a}}_{\mathrm{M}}(t)$ at the surface of the bacteria ($c^{\mathrm{a}}_{\mathrm{M}}(t)$ will be determined in §2.2.2), and Eq. (2c) states that ML complex is not bioactive, i.e. not accumulated by the metal M-sensing bacteria. Following the procedure detailed elsewhere,[13,36] the exact solution of Eqs. (1)-(2) can be written in the form

$$\begin{cases} \overline{c}_{\mathrm{M}}(r,t) = 1 - \dfrac{a}{r}\left[1 - \overline{c}^{\mathrm{a}}_{\mathrm{M}}(t)\right] \dfrac{\varepsilon \overline{K}_{\mathrm{ML}}\left[\mathrm{e}^{\overline{h}_{\mathrm{a}}(1-r/a)} - (1-\alpha)\mathrm{e}^{-\overline{h}_{\mathrm{a}}(1-r/a)}\right] + \left[\alpha + \overline{h}_{\mathrm{a}}(2-\alpha)\right](1 - \varphi^{1/3} r/a)}{\alpha\varepsilon\overline{K}_{\mathrm{ML}} + \left[\alpha + \overline{h}_{\mathrm{a}}(2-\alpha)\right](1-\varphi^{1/3})} & \text{(a)} \\ \overline{c}_{\mathrm{ML}}(r,t) = 1 - \dfrac{a}{r}\left[1 - \overline{c}^{\mathrm{a}}_{\mathrm{M}}(t)\right] \dfrac{\left[\alpha + \overline{h}_{\mathrm{a}}(2-\alpha)\right](1 - \varphi^{1/3} r/a) - \left[\mathrm{e}^{\overline{h}_{\mathrm{a}}(1-r/a)} - (1-\alpha)\mathrm{e}^{-\overline{h}_{\mathrm{a}}(1-r/a)}\right]}{\alpha\varepsilon\overline{K}_{\mathrm{ML}} + \left[\alpha + \overline{h}_{\mathrm{a}}(2-\alpha)\right](1-\varphi^{1/3})} & \text{(b)} \end{cases} \tag{3}$$

where we introduced the dimensionless concentrations $\overline{c}_{i=\mathrm{M,ML}}(r,t) = c_{i=\mathrm{M,ML}}(r,t) / c^{*}_{i=\mathrm{M,ML}}(t)$ and $\overline{c}^{a}_{\mathrm{M}}(t) = c^{a}_{\mathrm{M}}(t) / c^{*}_{\mathrm{M}}(t)$, and the scalar $\alpha = 1 - \mathrm{e}^{2\overline{h}_{\mathrm{a}}\left(1-\varphi^{-1/3}\right)}$ with $\overline{h}_{\mathrm{a}}$ (dimensionless) defined by

$$\overline{h}_{\mathrm{a}} = \sqrt{\overline{\kappa}_{\mathrm{a}}} \sqrt{1 + 1/\left(\varepsilon \overline{K}_{\mathrm{ML}}\right)} \tag{4}$$

The Damköhler number $\overline{\kappa}_{\mathrm{a}} = k_{\mathrm{a}} c^{*}_{\mathrm{L}} a^2 / D_{\mathrm{M}}$ in Eq. (4) can be seen as the dimensionless rate constant of ML formation which compares the steady state M diffusional timescale, $\tau_{\mathrm{SS}} = a^2 / D_{\mathrm{M}}$, with the reaction timescale $1/\left(k_{\mathrm{a}} c^{*}_{\mathrm{L}}\right)$. Equivalently, $\sqrt{\overline{\kappa}_{\mathrm{a}}}$ compares a with the thickness μ_{o} of the so-called reaction layer (**Figure 1**) defined by $\mu_{\mathrm{o}} = \sqrt{D_{\mathrm{M}} / \left(k_{\mathrm{a}} c^{*}_{\mathrm{L}}\right)}$, which represents the distance travelled by a free metal ion via diffusion before it re-associates with L to form ML. The supply flux of M to the biosensor surface, denoted as J_{M} (mol m^{-2} s^{-1}), is given at time *t* by $J_{\mathrm{M}}(t) = D_{\mathrm{M}}\left(\partial c_{\mathrm{M}}(r,t) / \partial r\big|_{r=a}\right)$. Using Eq. (3a), the result can be recast in the concise form

$$J_{\mathrm{M}}(t) = p_{\mathrm{ML}} D_{\mathrm{M}}\left[c^{*}_{\mathrm{M}}(t) - c^{\mathrm{a}}_{\mathrm{M}}(t)\right] / a \tag{5}$$

with $p_{ML} = p_o / \left(1-\varphi^{1/3}\right)$, and p_o is the (dimensionless) scalar defined by $p_o = 1 + \varepsilon \bar{K}_{ML} \xi$ which quantifies the contribution of ML to the M supply flux as a function of ML lability parameter ξ ($0 \le \xi \le 1$) defined by Duval et al.[13] (cf. Eq. (22) in Ref. [13]). In the limit $\varphi << 1$, ξ reduces to[13,36]

$$\xi \approx \sqrt{\bar{\kappa}_a} / \left(\sqrt{\bar{\kappa}_a} + \sqrt{\varepsilon \bar{K}_{ML}} \sqrt{1 + \varepsilon \bar{K}_{ML}} \right) \quad (6)$$

where $\varepsilon = D_{ML} / D_M$ is the ratio between diffusion coefficients of ML and M. In line with earlier conclusion,[13,37] the parameter ξ in the dilute limit is independent of the boundary condition adopted at the surface of the M-consuming interfaces, i.e. on $c_M^a(t)$.

As detailed elsewhere,[11,13,15] criteria can be established to distinguish the nature of the contribution (if any) of ML to the M supply flux, J_M, depending on ML lability parameter ξ. For the sake of completeness and clarity, we recall briefly below the basic arguments. At the level of the (volume) reaction M+L↔ML in solution, discrimination needs to be made first between *dynamic* and *inert* complexes on the basis of the comparison between the characteristic lifetimes of M (given by $1 / k_a c_L^*$) and ML ($1 / k_d$) and timescale (τ_{SS}) for the steady state M diffusion from solution to the biosensor surface. In detail, ML is *dynamic* in the time window τ_{SS} with a resulting fast interconversion between M and ML if

$$k_a c_L^* \tau_{SS} >> 1 \text{ and } k_d \tau_{SS} >> 1 \quad (7)$$

and ML is *inert* if

$$k_a c_L^* \tau_{SS} << 1 \text{ and } k_d \tau_{SS} << 1 \quad (8)$$

In the latter case, ML does *not* contribute in any way to the M supply flux at the biosensor surface. For *dynamic* complexes, different scenarios can be defined from the analysis of the J_M-flux property under sink metal condition (i.e. $c_M^a \equiv 0$), which comes to *qualify the maximal ML contribution to* J_M *within the diffusion timescale* τ_{SS}. Namely, for $\bar{\kappa}_a \to 0$ (i.e. $\xi \to 0$ and $p_o \to 1$), the flux $J_M(t)$ reduces to $J_M(t) = D_M c_M^*(t) / a$: this is the situation where the only free metal M is relevant to the supply flux, and ML behaves as if it is inert on the timescale of M diffusion. The other extreme $\bar{\kappa}_a >> 1$ (equivalent to the condition $k_a c_L^* \tau_{SS} >> 1$) refers to dynamic ML complexes, and two limiting situations can be distinguished depending on the nature of the ML contribution to the flux. In detail, for $\bar{\kappa}_a >> \left(\varepsilon \bar{K}_{ML}\right)\left(1 + \varepsilon \bar{K}_{ML}\right)$, we have $\xi \to 1$ (cf. Eq. (6)) and $p_o \to 1 + \varepsilon K_{ML}$, and J_M then simplifies into $J_M(t) = \bar{D}(t) c_{M,t}^*(t) / a$, where $\bar{D}(t) = \left[D_M c_M^*(t) + D_{ML} c_{ML}^*(t) \right] / c_{M,t}^*(t)$ ($m^2\ s^{-1}$) is the concentration-averaged diffusion coefficient of M

and ML at *t* with $c^*_{\mathrm{M,t}}(t)$ the total metal concentration (mol m^{-3}) in bulk solution defined by $c^*_{\mathrm{M,t}}(t) = c^*_{\mathrm{M}}(t)\left(1+\bar{K}_{\mathrm{ML}}\right)$: this is the *fully labile* ML case where ML contribution to the flux is of a purely diffusive nature, with the equilibrium between M and ML being maintained at any position r in the diffusion layer. For $\bar{\kappa}_{\mathrm{a}} << \left(\varepsilon\bar{K}_{\mathrm{ML}}\right)\left(1+\varepsilon\bar{K}_{\mathrm{ML}}\right)$ - which implies the inequality $\varepsilon\bar{K}_{\mathrm{ML}} >> 1$ so as to satisfy the examined limit $\bar{\kappa}_{\mathrm{a}} >> 1$ - the expressions of ξ and $J_{\mathrm{M}}(t)$ reduce to $\xi \to \sqrt{\bar{\kappa}_{\mathrm{a}}}/\left(\varepsilon\bar{K}_{\mathrm{ML}}\right)$ (i.e. $p_{\mathrm{o}} \to 1+\sqrt{\bar{\kappa}_{\mathrm{a}}}$) and $J_{\mathrm{M}}(t) = D_{\mathrm{M}}c^*_{\mathrm{M}}(t)/a + J_{\mathrm{kin}}(t)$ with $J_{\mathrm{kin}}(t) = k_{\mathrm{d}}c^*_{\mathrm{ML}}(t)\mu_{\mathrm{o}}$: this is the *nonlabile* ML case where M bioaccumulation is dictated by the diffusion of free M *and* the kinetics of ML dissociation at the surface of the M-accumulating bacteria.

2.2.2. Expressions for the metal biouptake flux, and the time-dependent concentrations of free metal species in bulk solution, at the surface and in the intracellular body of the metal-accumulating bacteria.

The uptake of free M by the bacteria is assumed to follow a Michaelis-Menten mechanism, which corresponds to a fast langmuirian adsorption of M at the membrane transporter sites distributed over the entire surface of the bacteria, followed by a rate-limiting internalisation step with kinetic constant k_{int} (s^{-1}).[11,12,15,30,38] In studies on metal monitoring by bacterial reporters, the linear Henry regime for metal bioaccumulation is relevant as it corresponds to a low coverage of the internalisation sites by M and to an ensuing linearity between bioluminescence at *t* and bioavailable metal concentration (cf. §3).[23] In this regime, the M biouptake flux $J_{\mathrm{u}}(t)$ reads as[11,12,15,30]

$$J_{\mathrm{u}}(t) = K_{\mathrm{H}}k_{\mathrm{int}}c^a_{\mathrm{M}}(t) \tag{9}$$

with K_{H} (m) the Henry adsorption constant. Under steady state conditions, the metal supply flux J_{M} defined by Eq. (5) must equate at any *t* the difference between internalisation and excretion fluxes

$$J_{\mathrm{M}}(t) = J_{\mathrm{u}}(t) - k_{\mathrm{e}}\phi_{\mathrm{M}}(t) \tag{10}$$

, where $J_{\mathrm{u}}(t)$ is given by Eq. (9), and $\phi_{\mathrm{M}}(t)$ (mol m^{-2}) is the concentration of intracellular free M at time *t* per microorganism surface area (cf. §2.1). The derivative of ϕ_{M} with respect to time corresponds to the uptake flux $J_{\mathrm{u}}(t)$ corrected for M excretion and conversion of internalized M into MP_{reg}, i.e.

$$\mathrm{d}\phi_{\mathrm{M}}(t)/\mathrm{d}t = J_{\mathrm{u}}(t) - k_{\mathrm{e}}\phi_{\mathrm{M}}(t) - k^*_{\mathrm{a,i}}\rho_{\mathrm{s}}\phi_{\mathrm{M}}(t) + k^*_{\mathrm{d,i}}\phi_{\mathrm{c}}(t) \tag{11}$$

where $k^*_{\mathrm{a,i}}$ and $k^*_{\mathrm{d,i}}$ were defined in §2.1, $\phi_{\mathrm{c}}(t)$ (mol m^{-2}) is the concentration of intracellular MP_{reg} complex at *t* per unit cell surface area, and ρ_{s} is the molar concentration of metal binding sites carried by P_{reg} and smeared-out over the volume V_{B} of a bacterium. The counterpart of Eq. (11) for $\phi_{\mathrm{c}}(t)$ is written

$$\mathrm{d}\phi_{\mathrm{c}}(t)/\mathrm{d}t = k_{\mathrm{a,i}}^{*}\rho_{\mathrm{s}}\phi_{\mathrm{M}}(t) - k_{\mathrm{d,i}}^{*}\phi_{\mathrm{c}}(t) \tag{12}$$

Finally, at any *t*, the level of metal depletion in bulk solution is determined by the amount of accumulated and excreted free M according to the following mass balance condition

$$\int_{a}^{r_{\mathrm{c}}} r^{2}\left\{\left[c_{\mathrm{M}}(r,t)+c_{\mathrm{ML}}(r,t)\right]-\left[c_{\mathrm{M}}(r,0)+c_{\mathrm{ML}}(r,0)\right]\right\}\mathrm{d}r = -a^{2}\int_{0}^{t}\left[J_{\mathrm{u}}(t)-k_{\mathrm{e}}\phi_{\mathrm{M}}(t)\right]\mathrm{d}t \tag{13}$$

where the M and ML concentration profiles, $c_{\mathrm{M,ML}}(r,t)$, are defined by Eq. (3).

The set of Eqs. (9)-(13) defines the time-dependent concentration of M in bulk solution and at the biosensor/solution interface ($c_{\mathrm{M}}^{*}(t)$ and $c_{\mathrm{M}}^{\mathrm{a}}(t)$, respectively), and the concentrations of intracellular M and $\mathrm{MP_{reg}}$ ($\phi_{\mathrm{M}}(t)$ and $\phi_{\mathrm{c}}(t)$, respectively) using the boundary conditions $\phi_{\mathrm{M}}(t=0)=\phi_{\mathrm{c}}(t=0)=0$. After some algebra and recourse to Laplace transform, it can be demonstrated that the bulk M concentration at any time *t*, $c_{\mathrm{M}}^{*}(t)$, is determined by the following explicit expression

$$c_{\mathrm{M}}^{*}(t)/c_{\mathrm{M}}^{*,0} = c_{\mathrm{M}}^{*,\infty}/c_{\mathrm{M}}^{*,0} - f_{+}\mathrm{e}^{-\bar{\omega}_{+}\bar{t}} + f_{-}\mathrm{e}^{-\bar{\omega}_{-}\bar{t}} \tag{14}$$

where $c_{\mathrm{M}}^{*,0}=c_{\mathrm{M}}^{*}(t=0)$, $c_{\mathrm{M}}^{*}(t\to\infty)=c_{\mathrm{M}}^{*,\infty}$, $\bar{t}=t/\tau_{\mathrm{a,i}}$ is the dimensionless timescale with $\tau_{\mathrm{a,i}}=1/\left(k_{\mathrm{a,i}}^{*}\rho_{\mathrm{s}}\right)$ the lifetime of intracellular free metal M, and $\bar{K}_{\mathrm{i}}=\tau_{\mathrm{d,i}}/\tau_{\mathrm{a,i}}$ is the stability constant of $\mathrm{MP_{reg}}$ complex with $\tau_{\mathrm{d,i}}=1/k_{\mathrm{d,i}}^{*}$ the lifetime of $\mathrm{MP_{reg}}$. The dimensionless factors $f_{\pm}$ involved in Eq. (14) are further defined by

$$f_{\pm} = \frac{\left[\lambda_{\mathrm{o}}-\left(\bar{\omega}_{\pm}\bar{\tau}_{\mathrm{o}}\right)^{-1}\right]\left[1+\bar{K}_{\mathrm{i}}\left(1-\bar{\omega}_{\pm}\right)\right]}{\left(1-\lambda_{\mathrm{o}}\right)\bar{K}_{\mathrm{i}}\left(\bar{\omega}_{-}-\bar{\omega}_{+}\right)} \tag{15}$$

where the (dimensionless) frequencies $\bar{\omega}_{\pm}$ in Eq. (15) are given by

$$\bar{\omega}_{\pm} = \frac{1}{2}\left(1+\frac{\zeta}{\bar{\tau}_{\mathrm{o}}}+\frac{1}{\bar{K}_{\mathrm{i}}}\right)\left(1\pm\sqrt{1-4\frac{\bar{K}_{\mathrm{i}}}{\bar{\tau}_{\mathrm{o}}}\left(\zeta+\bar{K}_{\mathrm{i}}\right)\left[1+\bar{K}_{\mathrm{i}}\left(1+\frac{\zeta}{\bar{\tau}_{\mathrm{o}}}\right)\right]^{-2}}\right) \tag{16}$$

The (dimensionless) timescale $\bar{\tau}_{\mathrm{o}}$ involved in Eqs. (15)-(16) is defined by $\bar{\tau}_{\mathrm{o}}=\tau_{\mathrm{o}}/\tau_{\mathrm{a,i}}$ with the time constant τ_{o} (s) given by

$$\tau_{\mathrm{o}} = \left(1+\bar{K}_{\mathrm{ML}}\right)\left(\frac{a}{K_{\mathrm{H}}k_{\mathrm{int}}}\right)\left[1+\left(p_{\mathrm{ML}}Bn\right)^{-1}\left(1-f_{\mathrm{a,M}}\right)\right]\frac{1-\varphi}{3\varphi} \tag{17}$$

while the dimensionless scalars ζ and λ_{o} appearing in Eqs. (15)-(16) read as

$$\zeta = 1+\left(1+\bar{K}_{\mathrm{ML}}\right)\left(\frac{ak_{\mathrm{e}}}{K_{\mathrm{H}}k_{\mathrm{int}}}\right)\frac{1-\varphi}{3\varphi} \tag{18}$$

$$\lambda_{\mathrm{o}} = \left\{1-\left[1+\left(p_{\mathrm{ML}}Bn\right)^{-1}\right]/\left[\left(p_{\mathrm{ML}}Bn\right)^{-1}f_{\mathrm{a,M}}\right]\right\}^{-1} \tag{19}$$

315 , respectively. The physical meanings of τ_o and ζ are thoroughly discussed in §2.2.3, together with the
316 implications of Eq. (14) in terms of dynamics of metal bioaccumulation. Eq. (16) is obviously meaningful
317 for values of $\overline{K}_i$, ζ and $\overline{\tau}_o$ in line with a positive argument of the square root in Eq. (16) : a Taylor-series
318 expansion of that argument with respect to φ for the here-considered case of dilute cell suspension (
319 $\varphi << 1$) evidences that positivity of that argument is always verified. In Eqs. (17) and (19), Bn is the so-
320 called Bosma number[39] that compares the M diffusion conductance, $a^{-1}D_M$ (m s^{-1}), and the M
321 internalisation conductance $K_H k_{int}$ (m s^{-1})

322 $$Bn = a^{-1}D_M / \left(K_H k_{int}\right) \tag{20}$$

323 The extremes $Bn^{-1} << 1$ and $Bn^{-1} >> 1$ correspond to a metal bioaccumulation process that is rate-limited
324 by M internalisation kinetics and M diffusional transport, respectively. The (dimensionless) quantity $f_{a,M}$
325 in Eqs. (17) and (19) depends on the cell volume fraction φ according to Eq. S1 given in **SI**†. For $\varphi << 1$, it
326 can be shown that $f_{a,M}$ simplifies into the following expression that involves the ML lability parameter ξ
327 defined by Eq. (6)

328 $$f_{a,M} \approx 2^{-1}\varphi^{1/3}\left(1 + \varepsilon\overline{K}_{ML}\xi\right) / \left(1 + \varepsilon\overline{K}_{ML}\right) \tag{21}$$

329 At $t \to \infty$, the partitioning of free M between the solution and the intracellular volume of the bacteria
330 is fully equilibrated, and the resulting bulk metal concentration $c_M^*\left(t \to \infty\right) = c_M^{*,\infty}$ involved in Eq. (14) can
331 be written in the concise dimensionless form

332 $$c_M^{*,\infty} / c_M^{*,0} = \left[1 + \frac{1 + \overline{K}_i}{1 + \overline{K}_{ML}}\left(\frac{3\varphi}{1-\varphi}\frac{K_H k_{int}}{a k_e}\right)\right]^{-1}\left(1 - \frac{\left(p_{ML}Bn\right)^{-1}}{1 + \left(p_{ML}Bn\right)^{-1}} f_{a,M}\right) \tag{22}$$

333 Given the expression (14) that defines $c_M^*\left(t\right)$, using Eq. (10) we finally infer that the concentration of M
334 at the cell surface, $c_M^a\left(t\right)$, and the metal biouptake flux $J_u\left(t\right)$ (Eq. (9)) are formulated according to

335 $$c_M^a\left(t\right) = \frac{J_u\left(t\right)}{K_H k_{int}} = \frac{1}{1 + \left(p_{ML}Bn\right)^{-1}}\left[c_M^*\left(t\right) + \left(p_{ML}Bn\right)^{-1} k_e \phi_M\left(t\right) / \left(k_{int}K_H\right)\right] \tag{23}$$

336 For the sake of completeness, we report in **SI**† the expressions obtained for the surface concentration of
337 M at equilibrium, denoted as $c_M^a\left(t \to \infty\right) = c_M^{a,\infty}$, and for the intracellular concentrations of free and
338 complexed metal, i.e. $\phi_M\left(t\right)$ and $\phi_c\left(t\right)$, respectively (cf. Eqs. (S2)-(S5) in **SI**†).
339
340 *2.2.3. Bulk metal depletion: timescales and equilibrium situation.*

Equation (14) highlights that the bulk concentration $c_{\mathrm{M}}^{*}(t)$ of free metal M decreases over time according to 2 exponential functions with associated timescales $\tau_{\pm}$ defined by $\tau_{\pm}=\tau_{\mathrm{a,i}}\bar{\omega}_{\pm}^{-1}$ where $\bar{\omega}_{\pm}$ are given by Eq. (16) that involves the time constant τ_{o} defined by Eq. (17). Interestingly, the decay of $c_{\mathrm{M}}^{*}(t)$ over time featured by Eq. (14) is similar to the double exponential form adopted in [40] to describe the time-dependence of bulk protein concentration following protein adsorption and uptake by spherical resin beads. Realizing that $\tau_{+}<\tau_{-}$, τ_{+} and τ_{-} feature the short- and long-term components of bulk M depletion, respectively. We provide below a biophysical meaning of the processes having time constants $\tau_{\pm}$, and we identify the situations where bulk metal depletion kinetics is controlled by both τ_{+} and τ_{-}, or by only one of these two timescales.

Absence of M excretion. For poorly-metal excreting bacteria, i.e. when M internalization is much faster than excretion (i.e. $k_{\mathrm{e}}/k_{\mathrm{int}}\to 0$, or equivalently $\zeta\approx 1$, cf. Eq. (18)), it can be shown that the expressions of $\tau_{\pm}$ considered in the limits $\tau_{\mathrm{o}}/\tau_{\mathrm{a,i}}\ll 1$, $\tau_{\mathrm{o}}/\tau_{\mathrm{a,i}}\gg 1$, $\bar{K}_{\mathrm{i}}\ll 1$ (weak MP_{reg} complex) or $\bar{K}_{\mathrm{i}}\gg 1$ (strong MP_{reg} complex) reduce to

$$\begin{cases}\tau_{+}\approx \min\left(\left(\tau_{\mathrm{d,i}}^{-1}+\tau_{\mathrm{a,i}}^{-1}\right)^{-1},\tau_{\mathrm{o}}\right) & \text{(a)}\\ \tau_{-}\approx \max\left(\left(\tau_{\mathrm{d,i}}^{-1}+\tau_{\mathrm{a,i}}^{-1}\right)^{-1},\tau_{\mathrm{o}}\right) & \text{(b)}\end{cases} \tag{24}$$

The term $\left(\tau_{\mathrm{d,i}}^{-1}+\tau_{\mathrm{a,i}}^{-1}\right)^{-1}$ pertaining to one of the two kinetic components of bulk M depletion is determined by the only time constants $\tau_{\mathrm{a,i}}$ and $\tau_{\mathrm{d,i}}$ for the formation and dissociation of intracellular MP_{reg}, respectively, with the kinetic limits $\left(\tau_{\mathrm{d,i}}^{-1}+\tau_{\mathrm{a,i}}^{-1}\right)^{-1}\approx\tau_{\mathrm{d,i}}$ and $\left(\tau_{\mathrm{d,i}}^{-1}+\tau_{\mathrm{a,i}}^{-1}\right)^{-1}\approx\tau_{\mathrm{a,i}}$ applicable to weak and strong MP_{reg} complexes, respectively. In contrast, the time constant τ_{o} (Eq. (17)) relevant for the other component of the depletion process (Eq. (24)) is *independent* of the chemodynamic properties of MP_{reg}: it simply corresponds to the timescale for transferring M from bulk solution to the intracellular cell volume prior to its sequestration by P_{reg}. The relative contributions of the short and long-term components to the overall depletion process, as identified by Eq. (24) for $k_{\mathrm{e}}/k_{\mathrm{int}}\to 0$, depend on the respective magnitudes of f_{+} and f_{-} (Eq. (15)) involved in the definition of $c_{\mathrm{M}}^{*}(t)$ (Eq. (14)). Combining Eqs. (24) and (15) with $\tau_{\pm}=\tau_{\mathrm{a,i}}\bar{\omega}_{\pm}^{-1}$, we demonstrate that bulk M depletion for $k_{\mathrm{e}}/k_{\mathrm{int}}\to 0$ in the limits $\tau_{\mathrm{o}}/\tau_{\mathrm{a,i}}\ll 1$, $\tau_{\mathrm{o}}/\tau_{\mathrm{a,i}}\gg 1$, $\bar{K}_{\mathrm{i}}\ll 1$ or $\bar{K}_{\mathrm{i}}\gg 1$ *systematically* proceeds according to a *single* exponential decaying function of time with a single depletion time constant, denoted as τ_{depl}, that identifies with τ_{o}. The bulk M concentration can then be approximated by

$$c_{\mathrm{M}}^{*}(t)/c_{\mathrm{M}}^{*,0} \approx \left(1-c_{\mathrm{M}}^{*,\infty}/c_{\mathrm{M}}^{*,0}\right)\mathrm{e}^{-t/\tau_{\mathrm{depl}}} + c_{\mathrm{M}}^{*,\infty}/c_{\mathrm{M}}^{*,0} \quad (25)$$

where $c_{\mathrm{M}}^{*,\infty}/c_{\mathrm{M}}^{*,0}$ is defined by Eq. (22). Under the examined conditions, the presence of the intracellular metal binding ligand P_{reg} does not affect the kinetics of bulk M depletion nor the equilibrium bulk concentration of M, $c_{\mathrm{M}}^{*,\infty}/c_{\mathrm{M}}^{*,0}$. Indeed, regardless of the magnitude of $\overline{K}_{\mathrm{i}}$, $c_{\mathrm{M}}^{*,\infty}/c_{\mathrm{M}}^{*,0}$ necessarily tends to 0 value for bacterial systems where M excretion is insignificant, which is inferred from Eq. (22) taken in the limit $k_{\mathrm{e}}/k_{\mathrm{int}} \to 0$.

Presence of M excretion. When M efflux pumps are operational (i.e. $k_{\mathrm{e}}/k_{\mathrm{int}} \neq 0$), the resulting M excretion tends to *buffer* the concentration of M in solution so that the maximum level of depletion reached at $t \to \infty$ necessarily decreases as compared to the situation where excretion is not significant: this is in line with the increase of $c_{\mathrm{M}}^{*,\infty}/c_{\mathrm{M}}^{*,0}$ with increasing $k_{\mathrm{e}}/k_{\mathrm{int}}$ at given $\overline{K}_{\mathrm{i}}$, as formulated by Eq. (22). In addition, at fixed value of $k_{\mathrm{e}}/k_{\mathrm{int}}$, Eq. (22) evidences that $c_{\mathrm{M}}^{*,\infty}/c_{\mathrm{M}}^{*,0}$ now decreases with increasing $\overline{K}_{\mathrm{i}}$: M depletion at equilibrium is therefore enhanced by intracellular metal complexation process. The latter counteracts indeed the excretion-mediated buffering of bulk M concentration to an extent that depends on the ratio $\left(1+\overline{K}_{\mathrm{i}}\right)/\left(k_{\mathrm{e}}/k_{\mathrm{int}}\right)$ that is involved in Eq. (22).

For the case $k_{\mathrm{e}}/k_{\mathrm{int}} \neq 0$ or, equivalently, $\zeta > 1$ (cf. Eq. (18)), we report in **Table 1** the corresponding expressions of $\tau_{\pm}$ for the relevant limits $\tau_{\mathrm{o}}/\tau_{\mathrm{a,i}} << \zeta$, $\tau_{\mathrm{o}}/\tau_{\mathrm{a,i}} >> \zeta$, $\overline{K}_{\mathrm{i}} << 1$ and $\overline{K}_{\mathrm{i}} >> 1$ (Eqs. (26a,b), (27a), (28a,b) and (29a) in **Table 1,** respectively). These expressions constitute the analogues of Eq. (24) for cases where M excretion is significant. The obtained results are obviously more involved as the kinetics of metal depletion is now determined by the complex interplay between M excretion and internalisation (as subsumed in ζ), chemodynamics of MP_{reg} complex (via the time constants $\tau_{\mathrm{a,i}}$ and $\tau_{\mathrm{d,i}}$) and transfer of M from solution to bacterial body (via the time constant τ_{o}). The conditions underlying the applicability of a mono-exponential decrease of $c_{\mathrm{M}}^{*}(t)$ over time with associated depletion time constant τ_{depl} (Eq. (25)) are further identified in **Table 1** for each limit considered (Eqs. (26c,d), (27b,c), (28c) and (29b,c)) and the corresponding expressions of τ_{depl} are also specified. In particular, for $\overline{K}_{\mathrm{i}} << 1$, bulk M depletion kinetics is always captured by the single timescale $\tau_{\mathrm{depl}} \equiv \tau_{\mathrm{o}}/\zeta$, which is a factor $1/\zeta$ lower compared to that discussed above for the situation where M excretion is insignificant: excretion thus decreases the time required for M partitioning at the biointerface to reach equilibrium. In the extreme of infinitely fast excretion ($k_{\mathrm{e}} \to \infty$ or, equivalently, $\zeta \to \infty$), bulk M concentration is buffered so efficiently that

$c_{\mathrm{M}}^{*,\infty} / c_{\mathrm{M}}^{*,0} \approx 1$ (cf. Eqs. (21)-(22) for $\varphi \ll 1$), and M depletion then becomes insignificant. For strong P_{reg} complexant ($\bar{K}_{\mathrm{i}} \gg 1$) under conditions where the inequality $\bar{\tau}_{\mathrm{o}} / \zeta \gg 1$ is satisfied, e.g. for $k_{\mathrm{e}} \tau_{\mathrm{a,i}} \ll 1$ (cf. Eqs. (17) and (18)), τ_{depl} reduces to $\tau_{\mathrm{depl}} \approx 2\tau_{\mathrm{a,i}} / \left(1 - \sqrt{1 - 4/\bar{\tau}_{\mathrm{o}}}\right)$, which is independent of the excretion kinetic constant k_{e}. This is the situation where a sufficiently fast complexation of M by P_{reg} bypasses M excretion kinetics. The latter then becomes immaterial in defining the partitioning of M over time at the biosensor/medium interface. The possible existence of two timescales $\tau_{\pm}$ for bulk M depletion kinetics and the aforementioned contributions of M excretion and intracellular M complexation agree with conclusions by Duval et al.[19] and their numerical analysis of M partitioning at a metal-accumulating interface in the scenario where metal complexation in solution is not significant. In particular, we verified that Eq. (22) (or equivalently Eq. (30) reported below) in the limit $\bar{K}_{\mathrm{ML}} = 0$ (absence of metal-complexing ligand in solution) correctly reproduces the ratio $c_{\mathrm{M}}^{*,\infty} / c_{\mathrm{M}}^{*,0}$ evaluated in Ref. [19] under the conditions where cell electrostatics is screened and linear Henry bioaccumulation regime applies, i.e. $K_{\mathrm{M}} / c_{\mathrm{M}}^{\mathrm{a}}(t) \gg 1$ where K_{M} relates to the M affinity for the metal transporter sites at the bacterial membrane. Under such conditions, we further checked that the characteristic depletion frequencies $\bar{\omega}_{\pm}$ evaluated from Eq. (16) for strong P_{reg} complexant (i.e. $\bar{K}_{\mathrm{i}} \gg 1$) properly compare to values obtained from Eq. (36) in Ref. [19] valid for $\bar{K}_{\mathrm{i}} \gg 1$.

Effects of extracellular metal speciation and cell concentration on biointerfacial partitioning of metal species. The formulations obtained above for $c_{\mathrm{M}}^{*,\infty} / c_{\mathrm{M}}^{*,0}$ (Eq. (22)) and for the time constant τ_{o} (Eq. (17)) appearing in the defining expressions of both $\tau_{\pm}$ and τ_{depl} (cf. Eq. (24) and Eq. (26)-(29) in **Table 1**), evidence that bulk M depletion kinetics is intrinsically controlled by: (i) the nature of the process that limits the rate of metal bioaccumulation, as evidenced by the involvement of Bn^{-1} (Eq. (20)), (ii) the chemodynamics of intracellular MP_{reg} complex, via involvement of $\tau_{\mathrm{a,i}}$ and $\bar{K}_{\mathrm{i}}$, (iii) the efficiency of M internalisation compared to excretion, via involvement of the ratio $K_{\mathrm{H}} k_{\mathrm{int}} / (a k_{\mathrm{e}})$, (iv) the thermodynamics of extracellular metal speciation, via the dependence of Eqs. (16)-(22) on ML stability constant $\bar{K}_{\mathrm{ML}}$, and finally (v) the bioavailability of ML complex, via the lability parameter ξ which enters the definition of p_{ML} and $f_{\mathrm{a,M}}$ (cf. §2.2.1 and §2.2.2). Substituting the defining expressions of p_{ML} (cf. below Eq. (5)) and

Considered limit	**Corresponding expressions of $\tau_{\pm}$ and τ_{depl}**
$\tau_{\mathrm{o}}/\tau_{\mathrm{a,i}} \ll \zeta$	$\tau_{+} \approx \tau_{\mathrm{o}}/\zeta$ (a) $\tau_{-} \approx \tau_{\mathrm{d,i}}/\left(1+\bar{K}_{\mathrm{i}}/\zeta\right)$ (b) $\tau_{\mathrm{depl}} \equiv \begin{cases} \tau_{+} \text{ for } \left\lvert \dfrac{\bar{K}_{\mathrm{i}}(\zeta-1)}{\left(\bar{K}_{\mathrm{i}}+\zeta\right)\left(\lambda_{\mathrm{o}}\zeta-1\right)} \right\rvert \ll 1 \quad \text{(c)} \\ \tau_{-} \text{ for } \left\lvert \dfrac{\bar{K}_{\mathrm{i}}(\zeta-1)}{\left(\bar{K}_{\mathrm{i}}+\zeta\right)\left(\lambda_{\mathrm{o}}\zeta-1\right)} \right\rvert \gg 1 \quad \text{(d)} \end{cases}$ Eq. (26a-d)
$\tau_{\mathrm{o}}/\tau_{\mathrm{a,i}} \gg \zeta$	$\tau_{\pm} \approx 2\tau_{\mathrm{a,i}} \Big/ \left\{ \dfrac{1+\bar{K}_{\mathrm{i}}}{\bar{K}_{\mathrm{i}}} \left\{ 1 \pm \sqrt{\left(1 - \dfrac{4}{\bar{\tau}_{\mathrm{o}}} \left(\dfrac{\bar{K}_{\mathrm{i}}}{1+\bar{K}_{\mathrm{i}}} \right)^2 \right)} \right\} + \left[1 \pm \left(\dfrac{\bar{K}_{\mathrm{i}}-1}{1+\bar{K}_{\mathrm{i}}} \right) \Big/ \sqrt{\left(1 - \dfrac{4}{\bar{\tau}_{\mathrm{o}}} \left(\dfrac{\bar{K}_{\mathrm{i}}}{1+\bar{K}_{\mathrm{i}}} \right)^2 \right)} \right] \dfrac{\zeta}{\bar{\tau}_{\mathrm{o}}} \right\}$ (a) $\tau_{\mathrm{depl}} \equiv \begin{cases} \tau_{-} \approx \tau_{\mathrm{o}}/\zeta \quad \text{for } \bar{K}_{\mathrm{i}} \ll 1 \quad \text{(b)} \\ \tau_{-} \approx 2\tau_{\mathrm{a,i}} \Big/ \left(1 - \sqrt{1 - \dfrac{4}{\bar{\tau}_{\mathrm{o}}}} \right) \quad \text{for } \bar{K}_{\mathrm{i}} \gg 1 \quad \text{(c)} \end{cases}$ Eq. (27a-c)
$\bar{K}_{\mathrm{i}} \ll 1$	$\tau_{+} = \tau_{\mathrm{d,i}}$ (a) $\tau_{-} = \tau_{\mathrm{o}}/\zeta$ (b) $\tau_{\mathrm{depl}} \equiv \tau_{-}$ (c) Eq. (28a-c)
$\bar{K}_{\mathrm{i}} \gg 1$	$\tau_{\pm} \approx 2\tau_{\mathrm{a,i}} \Big/ \left\{ \left(1 \pm \sqrt{1 - \dfrac{4\bar{\tau}_{\mathrm{o}}}{\left(\bar{\tau}_{\mathrm{o}}+\zeta\right)^2}} \right) \left(1 + \dfrac{\zeta}{\bar{\tau}_{\mathrm{o}}} \right) + \dfrac{1}{\bar{K}_{\mathrm{i}}} \left[1 \pm \left(\dfrac{\bar{\tau}_{\mathrm{o}}-\zeta}{\bar{\tau}_{\mathrm{o}}+\zeta} \right) \Big/ \sqrt{1 - \dfrac{4\bar{\tau}_{\mathrm{o}}}{\left(\bar{\tau}_{\mathrm{o}}+\zeta\right)^2}} \right] \right\}$ (a) $\tau_{\mathrm{depl}} \equiv \begin{cases} \tau_{-} \approx 2\tau_{\mathrm{a,i}} \Big/ \left(1 - \sqrt{1 - 4/\bar{\tau}_{\mathrm{o}}} \right) \text{ for } \bar{\tau}_{\mathrm{o}} \gg \zeta \quad \text{(b)} \\ \tau_{-} \approx \tau_{\mathrm{a,i}}/\zeta \text{ for } \bar{\tau}_{\mathrm{o}} \ll \zeta \quad \text{(c)} \end{cases}$ Eq. (29a-c)

Table 1. Expressions of the time constants $\tau_{\pm} = \tau_{\mathrm{a,i}} \bar{\omega}_{\pm}^{-1}$ involved in the decay of bulk M concentration with time (Eq. (14)) within the limits specified in the left column where M excretion is accounted for (i.e. $k_{\mathrm{e}}/k_{\mathrm{int}} \neq 0$ or $\zeta > 1$ (Eq. (18)). The (dimensionless) frequencies $\bar{\omega}_{\pm}$ are defined by Eq. (16), and the timescale $\tau_{\mathrm{o}} = \bar{\tau}_{\mathrm{o}} \tau_{\mathrm{a,i}}$ (s) by Eq. (17). $\bar{K}_{\mathrm{i}} = \tau_{\mathrm{d,i}}/\tau_{\mathrm{a,i}}$ is the stability constant of intracellular MP_{reg} complex, with $\tau_{\mathrm{d,i}}$ and $\tau_{\mathrm{a,i}}$ the lifetimes of MP_{reg} and intracellular M, respectively. The conditions (if any) required for the existence of a single bulk M depletion timescale, τ_{depl}, are further specified wherever necessary together with corresponding expressions of τ_{depl}. See text for details.

$f_{\mathrm{a,M}}$ (Eq. (21)) into Eq. (22), we show that $c_{\mathrm{M}}^{*,\infty}/c_{\mathrm{M}}^{*,0}$ depends on the descriptors of processes (i)-(v) listed above according to the explicit expression valid for $\varphi \ll 1$

$$c_{\mathrm{M}}^{*,\infty}/c_{\mathrm{M}}^{*,0} \approx \left(1 - \frac{Bn^{-1}}{1+\left(1+\varepsilon\bar{K}_{\mathrm{ML}}\xi\right)^{-1} Bn^{-1}} \frac{\varphi^{1/3}}{2\left(1+\varepsilon\bar{K}_{\mathrm{ML}}\right)} \right) \Big/ \left(1 + \frac{3K_{\mathrm{H}}k_{\mathrm{int}}}{ak_{\mathrm{e}}} \frac{1+\bar{K}_{\mathrm{i}}}{1+\bar{K}_{\mathrm{ML}}} \varphi \right) \tag{30}$$

Similarly, substitution of p_{ML} and $f_{\mathrm{a,M}}$ into Eqs. (17)-(18) leads to the following expression of the timescale τ_{o}/ζ (which identifies to τ_{depl} for e.g. $\bar{K}_{\mathrm{i}} \ll 1$, cf. **Table 1**) in the dilute limit $\varphi \ll 1$

$$\tau_o / \zeta \approx \left\{1+\frac{Bn^{-1}}{1+\varepsilon\bar{K}_{ML}\xi}\left[1-\left(\frac{3/2+\varepsilon\bar{K}_{ML}(1+\xi/2)}{1+\varepsilon\bar{K}_{ML}}\right)\varphi^{1/3}\right]\right\} / \left(k_e+\frac{3K_H k_{int}}{a\left(1+\bar{K}_{ML}\right)}\varphi\right) \quad (31)$$

We discuss specifically in §2.2.4 how ML lability (ξ) and bioaccumulation kinetics (Bn^{-1}) impact M depletion thermodynamics and kinetics (Eqs. (30) and (31), respectively), and we analyse here the effects connected to M speciation in solution ($\bar{K}_{ML}$) and to changes in the cell volume fraction φ. Briefly, Eqs. (30)-(31) evidence that both $c_M^{*,\infty}/c_M^{*,0}$ and τ_o/ζ increase with increasing $\bar{K}_{ML}\left(=K_{ML}c_L^*\right)$ (up to leading-order terms in $\bar{K}_{ML}$) at fixed φ, meaning that extracellular metal complexation acts as a buffer of bulk M concentration. In turn, increasing K_{ML} at fixed concentration c_L^* of L (which is realized in practice by changing the nature of the ligand L) or increasing c_L^* at given K_{ML} leads to a reduction of M depletion at equilibrium and to an increase in the delay needed to achieve this equilibrium. The effects caused by extracellular M speciation on bulk M depletion are therefore opposite to those caused by intracellular M sequestration by P_{reg}. The retardation of the equilibrium situation upon increasing ML stability agrees with the conclusion by Pinheiro et al.[15] formulated for microorganisms devoid of intracellular M chelator (i.e. $\bar{K}_i \to 0$) in the absence of M excretion (i.e. $k_e \to 0$), and Eqs. (30)-(31) taken in these limits correctly reproduce Eqs. (13)-(14) given in Ref. [15] for media where L is absent (i.e. $\bar{K}_{ML} \to 0$). In addition, Eqs. (30)-(31) provide a rationale of the (intuitive) connections existing between the equilibrium level and kinetics of M depletion, and the concentration φ of biosensors, that is : $c_M^{*,\infty}/c_M^{*,0}$ decreases with increasing the amount of M-accumulating bacteria (cf. the leading order φ-term in Eq. (30)), and increasing φ fastens the depletion process (cf. Eq. (31)). Finally, we infer from Eq. (30) that the conditions marking a significant depletion of M from bulk solution can be formulated by the inequality $\varphi \geq \varphi^*$, where φ^* is the critical cell concentration that depends on the relevant parameters of the problem according to

$$\varphi^* = \frac{ak_e}{3K_H k_{int}}\frac{1+\bar{K}_{ML}}{1+\bar{K}_i} = \frac{a^2 k_e}{3D_M Bn^{-1}}\frac{1+\bar{K}_{ML}}{1+\bar{K}_i} \quad (32)$$

and the second equality in Eq. (32) follows directly from the definition of Bn^{-1} (Eq. (20)). The opposite roles played by the intra- and extracellular ligands L and P_{reg} in terms of effects on depletion at equilibrium are reflected by the ratio $\left(1+\bar{K}_{ML}\right)/\left(1+\bar{K}_i\right)$: the larger $\bar{K}_{ML}$ is, the higher is the concentration of bacteria required to deplete a given amount of M, and conversely for $\bar{K}_i$. The buffering of M concentration in solution by excretion process is also correctly captured by Eq. (32): the more efficient is excretion (i.e. k_e

466 is high), the larger becomes the concentration of bacteria needed to achieve a given M depletion level,
467 and conversely for high k_{int}.
468
469 *2.2.4. Metal bioavailability.*
470 The expressions of $c_{\mathrm{M}}^{*,\infty} / c_{\mathrm{M}}^{*,0}$ and $\tau_{\mathrm{o}} / \zeta$ given by Eqs. (30)-(31) depend on the ML lability parameter
471 ξ which qualifies and quantifies the nature and magnitude, respectively, of the contribution of ML
472 complex to the M bioaccumulation flux, with the differentiation between inert and dynamic ML ($\xi \approx 0$
473 and $\xi \neq 0$, respectively) and, if dynamic, between non-labile and fully labile ML ($\xi \approx \sqrt{\bar{\kappa}_{\mathrm{a}}} / \varepsilon \bar{K}_{\mathrm{ML}}$ and $\xi \approx 1$
474 , respectively), as explained in §2.2.1. The quantities $c_{\mathrm{M}}^{*,\infty} / c_{\mathrm{M}}^{*,0}$ and $\tau_{\mathrm{o}} / \zeta$ further reflect the extent to
475 which M bioaccumulation is kinetically determined by M internalisation and/or M diffusion process,
476 depending on the magnitude of the reciprocal of the Bosma number Bn^{-1} (Eq. (20)) compared to unity.
477 We summarize in **Figure 2** all conditions invoked in §2.2.1 that must be verified for ML complex to be
478 inert, dynamic, and non-labile or fully labile, while replacing them in the relevant limits $Bn^{-1} << 1$ and
479 $Bn^{-1} >> 1$ where biouptake is controlled by M internalisation and M diffusion, respectively. For each case
480 considered across the spectrum of speciation and bioaccumulation dynamic scenarios, we report the
481 corresponding limits of Eqs. (30)-(31) pertaining to $c_{\mathrm{M}}^{*,\infty} / c_{\mathrm{M}}^{*,0}$ and $\tau_{\mathrm{o}} / \zeta$ (Eqs. (33a,b)-(36a,b) in **Figure 2**).
482 **Figure 2** thus extends the results by Pinheiro et al.[15] valid under the strict conditions where metal
483 excretion and intracellular metal complexation were ignored, and they provide a so-far missing overview
484 of the expressions that govern metal depletion over time for all relevant limits of speciation and
485 bioaccumulation dynamics.
486 For internalization-controlled bioaccumulation ($Bn^{-1} << 1$, case ❶ in **Figure 2**, Eqs. (33a,b)), there is
487 no limitation of the biouptake by M diffusion, the only free M concentration is relevant to the biouptake
488 and L simply acts as a buffer for the free M concentration in solution (§2.2.3). This is the conventional
489 situation treated by BLM where the surface concentration of M, $c_{\mathrm{M}}^{\mathrm{a}}$, is *a priori* assumed to equate with
490 the bulk M concentration, c_{M}^{*}, which actually corresponds to Eq. (23) taken in the limit $Bn^{-1} \to 0$. In
491 situations where bioaccumulation rate is limited by M diffusion ($Bn^{-1} >> 1$), the extent of ML dissociation
492 within the timescale τ_{ss} for steady state diffusion of M to the biosensor surface becomes relevant to
493 discriminate inert from dynamic ML complexes. The conditions fulfilled by inert and dynamic ML are then
494 formulated by Eqs. (7) and (8). For inert ML (case ❷ in **Figure 2**, Eqs. (34a,b)), expressions of $c_{\mathrm{M}}^{*,\infty} / c_{\mathrm{M}}^{*,0}$
495 and $\tau_{\mathrm{o}} / \zeta$ basically merge (up to leading order terms in φ) with those derived for case ❶ on the premise

that there is no concentration gradient at the biosurface, i.e. $c_M^* = c_M^a$ or, equivalently, $Bn^{-1} \to 0$. For dynamic ML (corresponding to $\bar{\kappa}_a >> 1$) the distinction between non-labile and fully labile ML complex (cases ❸ and ❹, respectively) is tied to the applicability of the inequalities $1 << \bar{\kappa}_a << \left(\varepsilon \bar{K}_{ML}\right)\left(1+\varepsilon \bar{K}_{ML}\right)$ and $\bar{\kappa}_a >> \left(\varepsilon \bar{K}_{ML}\right)\left(1+\varepsilon \bar{K}_{ML}\right)$, respectively. The contribution of non-labile ML to bulk M depletion and M transport is dominated by ML dissociation kinetics (case ❸, Eqs. (35a,b)). In the limit of fully labile ML, ML dissociation kinetics is so fast that the contribution of ML to M bioaccumulation flux is entirely governed by ML diffusion from bulk solution to the M-accumulating biointerface.

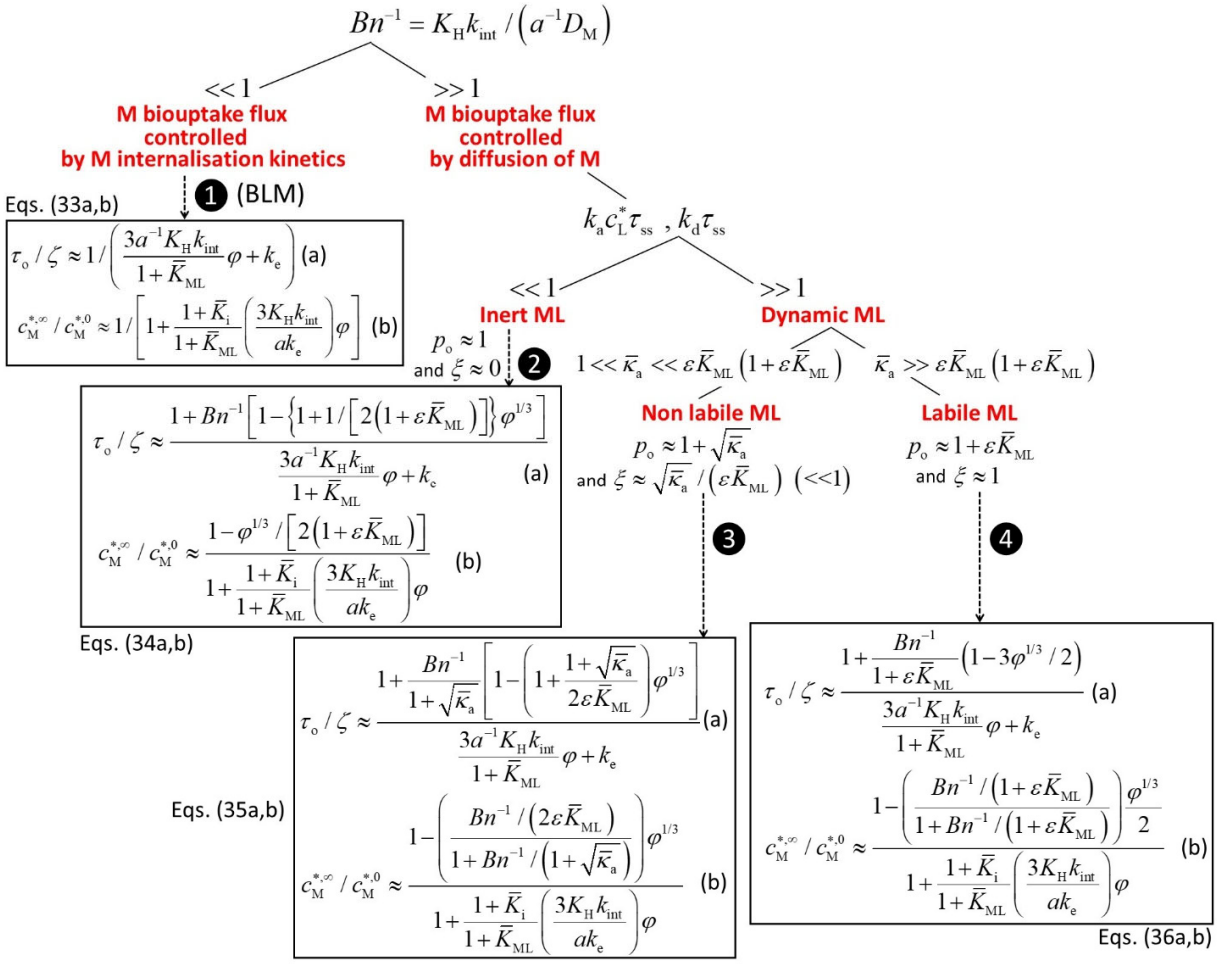

Figure 2. Conditional applications of the possible scenarios in terms of dynamics of metal bioaccumulation, and related contribution of ML complex to M biouptake flux (J_u). Scenario ❶ applies when bioaccumulation is limited by M internalisation kinetics without any resulting ML contribution to J_u. Scenario ❷, ❸ and ❹ refer to cases where M bioaccumulation is limited by M diffusion from bulk medium to the biosensor surface. More specifically, unlike cases ❸ and ❹, case ❷ is that where ML does not contribute to the M biouptake flux (inert ML). In cases ❸ and ❹, the contribution of ML to J_u is determined by ML dissociation kinetics (non-labile ML) and ML diffusion (fully labile ML), respectively. For all cases, the expressions of $c_M^{*,\infty} / c_M^{*,0}$ are provided together with those defining the time constant τ_o / ζ which corresponds to the M depletion timescale for weak intracellular MP_{reg} (cf. **Table 2**).

The timescale $\tau_{SS} = a^2 / D_M$ in Figure 2 refers to the steady state diffusion of M from solution to the accumulating biointerface. The Biotic Ligand Model (BLM) assumes equilibrium between metal affinity in bulk medium and at the biosensor surface (i.e. $c_M^a(t) \equiv c_M^*(t)$, cf. Eq. (23) for $Bn^{-1} \to 0$), which corresponds to case ❶. All parameters are defined in the text and glossary of symbols. See text for details.

Using Eqs. (30)-(31), in **Figures 3A,B** we report computed variations of τ_o / ζ as a function of Bn^{-1} and ML lability ξ. For the sake of comparison, predictions from the relevant limiting expressions specified in **Figure 2** are further reported. With increasing Bn^{-1}, τ_o / ζ decreases at fixed ξ, meaning that it takes less time to deplete a given amount of M when switching from internalised-controlled to diffusion-controlled M biouptake, which is line with a faster biouptake process achieved by increasing Bn^{-1}. For diffusion-controlled M biouptake (i.e. $Bn^{-1} >> 1$), increasing ML lability ξ leads to a decrease in τ_o / ζ : M depletion thus becomes faster when the contribution of ML to the uptake flux increases, i.e. from the non-labile to fully labile ML situations. **Figure 3C** further illustrates the expected decrease of $c_M^{*,\infty} / c_M^{*,0}$ with increasing Bn^{-1} at fixed cell concentration or, equivalently, with increasing φ / φ^* (where φ^* is defined by Eq. (32)). The new feature is that the impact of ML lability ξ (which includes the variables $\varepsilon \bar{K}_{ML}$ and $\bar{\kappa}_a$, cf. Eq. (6)) on $c_M^{*,\infty} / c_M^{*,0}$ is very moderate, as judged from the similarity of the curve computed for $\xi = 0.5$ and those corresponding to the extremes of inert and fully labile ML complex (not shown). This result can be understood from inspection of Eqs. (30) and (34b)-(36b) where quantities $\varepsilon \bar{K}_{ML}$ and $\bar{\kappa}_a$ are systematically involved in φ-dependent terms that are much lower than unity. In turn, $c_M^{*,\infty} / c_M^{*,0}$ (Eq. (30)) basically reduces to the simple expression $c_M^{*,\infty} / c_M^{*,0} \approx \left(1 + \varphi / \varphi^*\right)^{-1}$ with $c_M^{*,\infty} / c_M^{*,0} = 1/2$ for $\varphi / \varphi^* = 1$, in agreement with **Figure 3C**.

The buffering of bulk M concentration by ligand L in solution (as explained in §2.2.3) is illustrated in **Figure 4A** and **Figure 4B** by the increase of τ_o / ζ and $c_M^{*,\infty} / c_M^{*,0}$ with increasing $\bar{K}_{ML}$ at fixed values of ξ and Bn^{-1}, respectively. **Figure 4** further reveals that the magnitude of this buffering effect is reduced as biouptake becomes increasingly controlled by M-transport (increasing values of Bn^{-1}), in line with the decrease captured by **Figures 3A,B** for τ_o / ζ when lability of ML increases. Finally, **Figures 3-4** support the consistency between the results derived on the basis of Eqs. (30)-(31) and those obtained with the approximate Eqs. (33)-(36) within their applicable ranges of Bn^{-1} and ξ values (cf. **Figure 2**).

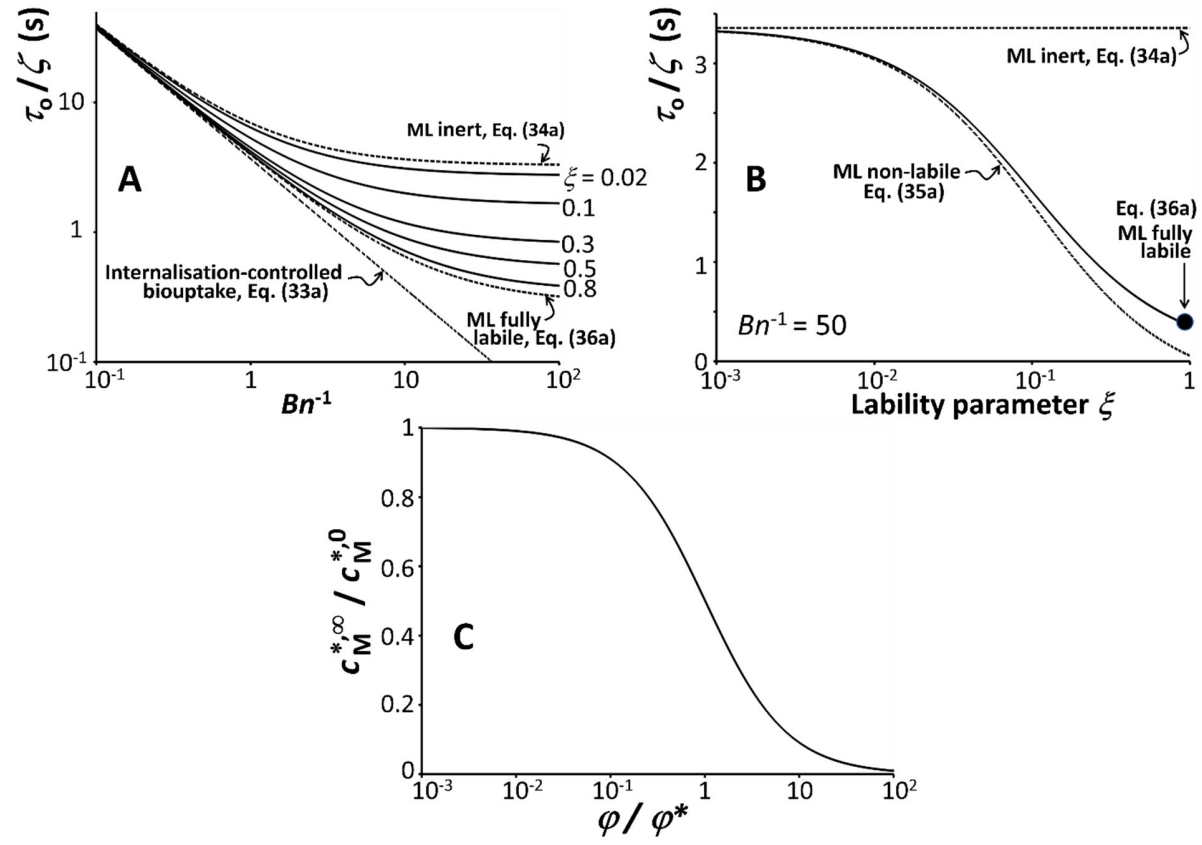

Figure 3. Variations of the time constant τ_o / ζ **(A,B)** and (dimensionless) bulk M concentration at equilibrium, $c_M^{*,\infty} / c_M^{*,0}$ **(C)** as a function of Bn^{-1} defined by Eq. (20) **(A),** ML lability parameter ξ (Eq. (6)) (**B**), and normalized cell volume fraction φ / φ^* where φ^* is given by Eq. (32) **(C)**. Model parameters if not specified in the figure: $\bar{K}_{ML} = 10$, $\varphi = 10^{-3}$, $\varepsilon = 1$, $a = 1$ μm, $D_M = 10^{-9}$ m^2 s^{-1}, $k_e = 0$ in **(A,B)**, $k_e = 10^{-4}$ s^{-1} and $\bar{K}_i = 10$ in **(C)**. The solid lines are predictions by Eq. (31) and Eq. (30) for τ_o / ζ **(A,B)** and $c_M^{*,\infty} / c_M^{*,0}$ **(C)**, respectively. Dotted lines refer to results obtained with the expressions of τ_o / ζ and $c_M^{*,\infty} / c_M^{*,0}$ given in Figure 2 for internalisation-controlled M biouptake, inert ML, non-labile ML and/or fully labile ML (specified in Figure 3). Orders of magnitude for selected values of φ, k_e and $\bar{K}_i$ conform to experimental data on Cd-excreting bacteria[16] and intracellular Cd complexation by metallothionein.[18]

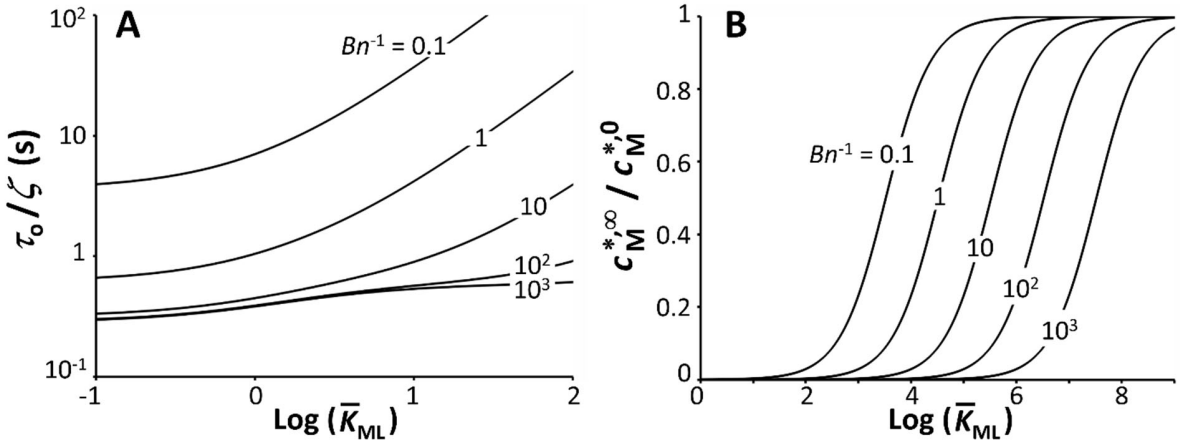

Figure 4. Variations of the time constant τ_o / ζ **(A)** and bulk M concentration at equilibrium $c_M^{*,\infty} / c_M^{*,0}$ **(B)** as a function of dimensionless ML stability constant, $\bar{K}_{ML} = K_{ML} c_L^*$, for different values of Bn^{-1} (indicated). Model parameters if not specified in the figure: $\varphi = 10^{-3}$, $\varepsilon = 1$, $a = 1$ μm, $D_M = 10^{-9}$ m² s⁻¹, $\xi = 0.5$, $k_e = 0$ **(A)** and $k_e = 10^{-3}$ s⁻¹ **(B)**, $\bar{K}_i = 10$ (only relevant in **(B)** because τ_o / ζ is independent of $\bar{K}_i$, cf. Eq. (31)). The solid lines are predictions by Eqs. (31) and (30) for τ_o / ζ and $c_M^{*,\infty} / c_M^{*,0}$, respectively.

3. Connections between metal partitioning dynamics at the biosensor/solution interface and bioluminescence signal.

3.1. Theoretical formulation.

In the situations where M depletion from solution is insignificant (i.e. for $\varphi << \varphi^*$), the bioluminescence $Lum^{(0)}$ (in counts s⁻¹) generated at time *t* by the bacterial metal sensors present at the (time-independent) concentration $c_B = \varphi / V_B$ can be written in the form[22]

$$Lum^{(0)}\left(t, c_M^{*,0}, \bar{c}_{B,p}(t)\right) = \psi \theta c_B \frac{K_H k_{int} c_M^{*,0} \left(1 - \tilde{K}_H S_a c_B\right)}{1 + \left(1 + \varepsilon \bar{K}_{ML} \xi\right)^{-1} Bn^{-1}} \left[F(t) \otimes \bar{c}_{B,p}(t)\right] \quad (37)$$

where the symbol $\otimes$ is the convolution product, and we recall that the initial bulk concentration of free M, $c_M^{*,0}$, obeys the relationship $c_M^{*,0} = c_{M,t}^{*,0} / \left(1 + \bar{K}_{ML}\right)$ where $c_{M,t}^{*,0}$ is the total bulk metal concentration (including M and ML species). We have specified in Eq. (37) that $Lum^{(0)}$ depends on time *t*, on the relevant bulk concentration of free metal, $c_M^{*,0}$, and on the dimensionless time-dependent concentration $\bar{c}_{B,p}(t)$ of *photoactive* cells, also termed *cell photoactivity*.[22] This concentration is defined by $\bar{c}_{B,p}(t) = c_{B,p}(t) / c_{B,p}^{max}$, where $c_{B,p}^{max}$ $\left(\leq c_B\right)$ is the maximum number density (in m⁻³) of photoactive bacteria the medium can sustain depending on the available resources therein required to convert internalized metal ions into light.

For medium compositions that exclude toxicity towards bacteria, $\overline{c}_{\mathrm{B,p}}(t)$ is an increasing sigmoid-like function of time,[21-23] independent of M concentration, with initial and end values $\overline{c}_{\mathrm{B,p}}(t=0)=0$ and $\overline{c}_{\mathrm{B,p}}(t\to\infty)=1$, respectively. Under such conditions, an increase in the total cell concentration c_{B} leads to an increase in the concentration of photoactive cells. As a first-order approximation, this connection is written in Eq. (37) according to the linear relationship $c_{\mathrm{B,p}}^{\max}=\theta c_{\mathrm{B}}$ with $0<\theta\leq 1$. We recall that the function $\overline{c}_{\mathrm{B,p}}(t)$, originally introduced in Ref. [22], is inspired by the modelling work of Delle Side et al.[41] on bacterial bioluminescence onset and quenching. In their work, these authors proposed a model to disentangle the roles of cell growth and quorum activation in shaping the bioluminescence signal produced constitutively by cells. In turn, adaptation of their treatment to metal-sensing bacteria[22] allows to differentiate between the total concentration of bacteria in the medium (taken here constant over time) and the time-dependent concentration of photoactive cells. Obviously, the physiological state of the bacteria is crucial in defining cell capacity to convert chemical information (e.g. the internalized M) into bioluminescence. This physiological state and the related cell metabolic activity at time *t* depend on the nutritional resources available in the medium. Both are effectively reflected by the magnitude of $\overline{c}_{\mathrm{B,p}}(t)$, with $\overline{c}_{\mathrm{B,p}}(t)=0$ and $\overline{c}_{\mathrm{B,p}}(t)=1$ pertaining to photoinactive and fully photoactive bacteria, respectively. As detailed elsewhere,[21] the quantity $\overline{c}_{\mathrm{B,p}}(t)$ may be equivalently interpreted as the (dimensionless) number of *photoactive cells* at time *t* with each of these cells maintaining a constant bioluminescence yield, or as a time-dependent bioluminescence yield that applies to *all* cells present in the medium.

The term $\left(1-\tilde{K}_{\mathrm{H}}S_{\mathrm{a}}c_{\mathrm{B}}\right)$ in Eq. (37) corrects the free metal concentration $c_{\mathrm{M}}^{*,0}$ for the amount of M that is passively adsorbed at the biosensor surface (this metal fraction does not contribute to the bioluminescence signal), with $\tilde{K}_{\mathrm{H}}$ (in m) the adsorption constant in the here-considered linear Henry adsorption regime. Passive metal adsorption at bacterial surfaces is usually fast compared to internalisation and M depletion,[15,16,30] which leads to a fast-initial decrease of bulk M concentration, in agreement with electroanalytical measurements[16] and formulation in Eq. (37). The resulting quadratic dependence of $Lum^{(0)}$ versus c_{B}, i.e. $Lum^{(0)}\sim c_{\mathrm{B}}\left(1-\tilde{K}_{\mathrm{H}}S_{\mathrm{a}}c_{\mathrm{B}}\right)$, has been validated by experimental data.[42] Eq. (37) holds for the practical case $t>>\tau_{\mathrm{q}}$, where *t* typically exceeds hours and τ_{q} (~min) is the characteristic duration of photon emission by luciferase-luciferin complexes.[22] In Eq. (37), ψ is defined by $\psi=S_{\mathrm{a}}V_{\mathrm{T}}k_{\nu}k_{\mathrm{f}}\tau_{\mathrm{q}}K_{\mathrm{Hi}}^{-1}$ (in counts s^{-1} mol^{-1} m^5), with S_{a} the surface area of an individual biosensor, k_{ν} (counts s^{-1} mol^{-1}) is the kinetic constant for photon emission per mole of luciferase, k_{f} (mol m^{-3} s^{-1}) is the kinetic

constant for luciferase production, and K_{Hi} (mol m^{-3}) is the Hill constant that relates to the affinity of the promoter for the $\mathrm{MP_{reg}}$ complex (**Figure 1**). The term $\frac{K_{\mathrm{H}} k_{\mathrm{int}} c_{\mathrm{M}}^{*,0}}{1+\left(1+\varepsilon \bar{K}_{\mathrm{ML}} \xi\right)^{-1} Bn^{-1}}$ in Eq. (37) simply corresponds to the steady state M biouptake flux in the absence of metal excretion (cf. Eq. (23) taken at t = 0). The dimensionless function $F(t)$ in Eq. (37) is defined by Eq. (16) in our previous report[22] and it reflects the rate of variation of luciferase concentration with time, which is mediated by the dynamics of M partitioning at the biosensor/solution interface and by the kinetics of the intracellular processes leading to the expression of the reporter gene (*lux*). For practical situations of strong intracellular metal-chelators $\mathrm{P_{reg}}$ ($\bar{K}_{\mathrm{i}} >> 1$) that significantly bypass M excretion (i.e. $k_{\mathrm{e}} \tau_{\mathrm{a,i}} << 1$) and for $k_{\mathrm{r}} \tau_{\mathrm{a,i}} << 1$ with k_{r} (s^{-1}) the effective kinetic constant associated with the inhibition of luciferase production and/or activity, we have[22]

$$F(t) \approx \left(1 - k_{\mathrm{eff}} / k_{\mathrm{r}}\right)^{-1} \left[\mathrm{e}^{-k_{\mathrm{r}} t} - \left(k_{\mathrm{eff}} / k_{\mathrm{r}}\right) \mathrm{e}^{-k_{\mathrm{eff}} t} \right] \tag{38}$$

where k_{eff} (s^{-1}) is defined by $k_{\mathrm{eff}} = k_{\mathrm{e}} / \left\{ \bar{K}_{\mathrm{i}} \left[1 + \left(1 + \varepsilon \bar{K}_{\mathrm{ML}} \xi\right)^{-1} Bn^{-1} \right] \right\}$.[21]

Under conditions where bulk metal depletion is significant, i.e. for $\varphi \sim \varphi^*$ or $\varphi > \varphi^*$ (cf. §2.2.3), following the bioluminescence modeling scheme detailed elsewhere[22] and correcting it for the dependence of bulk M concentration on time, we straightforwardly obtain for the bioluminescence signal denoted as $Lum(t)$

$$Lum(t) = \psi \theta c_{\mathrm{B}} \frac{K_{\mathrm{H}} k_{\mathrm{int}} c_{\mathrm{M}}^{*,0} \left(1 - \tilde{K}_{\mathrm{H}} S_{\mathrm{a}} c_{\mathrm{B}}\right)}{1 + \left(1 + \varepsilon \bar{K}_{\mathrm{ML}} \xi\right)^{-1} Bn^{-1}} \left\{ F(t) \otimes \left[\left(\frac{c_{\mathrm{M}}^{*}(t)}{c_{\mathrm{M}}^{*,0}} \bar{c}_{\mathrm{B,p}}(t) \right) \right] \right\} \tag{39}$$

where the ratio $c_{\mathrm{M}}^{*}(t) / c_{\mathrm{M}}^{*,0}$ is defined by Eq. (14) whose limits are specified in **Figure 2** for the relevant scenarios differing in terms of M bioaccumulation and speciation dynamics. For $c_{\mathrm{M}}^{*}(t) / c_{\mathrm{M}}^{*,0} = 1$, Eq. (39) correctly reproduces the non-depletive situation covered by Eq. (37). In cases where M depletion kinetics is determined by a single time constant τ_{depl} (cf. Eq. (24) and **Table 1**), we argued that Eq. (25) reproduces correctly the time-variation of $c_{\mathrm{M}}^{*} / c_{\mathrm{M}}^{*,0}$. Then, substituting Eq. (25) into Eq. (39) we show that the expression of the bioluminescence signal $Lum(t)$ with account of bulk M depletion can be written

$$Lum(t) = Lum^{(0)}\left(t, c_{\mathrm{M}}^{*,\infty}, \bar{c}_{\mathrm{B,p}}(t)\right) + Lum^{(0)}\left(t, c_{\mathrm{M}}^{*,0} - c_{\mathrm{M}}^{*,\infty}, \mathrm{e}^{-t/\tau_{\mathrm{depl}}} \bar{c}_{\mathrm{B,p}}(t)\right) \tag{40}$$

where $Lum^{(0)}(t,x,y)$ is given by Eq. (37), and x and y are dummy arguments referring to bulk M concentration and cell photoactivity, respectively. Equation (40) explains how the bioluminescence signal $Lum(t)$ is impacted by the kinetic and thermodynamic determinants of bulk metal depletion. Namely,

596 $Lum(t)$ can be viewed as the sum of two terms: the first term, $Lum^{(0)}\left(t, c_{\mathrm{M}}^{*,\infty}, \overline{c}_{\mathrm{B,p}}(t)\right)$, corresponds to the
597 bioluminescence signal that would be obtained in the absence of M depletion but with setting the bulk M
598 concentration to $x = c_{\mathrm{M}}^{*,\infty}$ and the (time-dependent) cell photoactivity to $y = \overline{c}_{\mathrm{B,p}}(t)$, while the second
599 term $Lum^{(0)}\left(t, c_{\mathrm{M}}^{*,0} - c_{\mathrm{M}}^{*,\infty}, \mathrm{e}^{-t/\tau_{\mathrm{depl}}}\overline{c}_{\mathrm{B,p}}(t)\right)$ pertains to the signal in the absence of M depletion with
600 $x = c_{\mathrm{M}}^{*,0} - c_{\mathrm{M}}^{*,\infty}$ and $y = \mathrm{e}^{-t/\tau_{\mathrm{depl}}}\overline{c}_{\mathrm{B,p}}(t)$. The underlying modifications of the bioluminescence signal due to
601 metal depletion are detailed in the next sections by analysing the dependence of $Lum(t)$ on cell volume
602 fraction and concentration of metal-binding ligand in solution.
603
604 **3.2. Effects of cell volume fraction on the bioluminescence signal** $Lum(t)$.

605 **Figures 5A,B** illustrate the changes of the bioluminescence signal caused by bulk M depletion upon
606 increasing cell volume fraction φ. The focus is given here on the analysis of the contribution of the ***only***
607 convolution product in Eq. (39). For that purpose, results in **Figures 5A,B** are reported in the dimensionless
608 form $\overline{Lum}(t) / \overline{Lum}_{\max}\Big|_{\varphi<<\varphi^*}$ with $\overline{Lum}(t) = Lum(t) / \left[c_{\mathrm{B}}\left(1 - \tilde{K}_{\mathrm{H}} S_{\mathrm{a}} c_{\mathrm{B}}\right)\right]$ and $\overline{Lum}_{\max}\Big|_{\varphi<<\varphi^*}$ is the maximum of
609 the bioluminescence signal $\overline{Lum}(t)$ reached in the absence of M depletion, i.e. at $\varphi << \varphi^*$. Accordingly,
610 the ratio $\overline{Lum}(t) / \overline{Lum}_{\max}\Big|_{\varphi<<\varphi^*}$ basically reflects the (normalized) bioluminescence produced *by a single*
611 *biosensor*. For the sake of demonstration, we adopt a *S*-shaped increase of the cell photoactivity $\overline{c}_{\mathrm{B,p}}(t)$
612 with time (red dotted curve in **Figures 5A,B**), and we introduce the characteristic timescales $\tau_{\mathrm{photoactivity}}$ and
613 τ_{biol} at which $\overline{c}_{\mathrm{B,p}}(t)$ features an inflexion point and deviates significantly from 0, respectively. As detailed
614 elsewhere, τ_{biol} marks the onset of bioluminescence increase with time and it is essentially controlled by
615 cell metabolism and nutritional quality of the medium.[21,23]

616 Starting from the situation $\varphi << \varphi^*$, increasing φ / φ^* leads to a decrease in bulk M concentration
617 from $c_{\mathrm{M}}^{*,0}$ to $c_{\mathrm{M}}^{*,\infty}$ within the period $\sim \tau_{\mathrm{depl}}$ (**Figure 5A**). If this depletion is completed before cells become
618 photoactive, i.e. for $\tau_{\mathrm{depl}} / \tau_{\mathrm{biol}} << 1$, the second term in Eq. (40) is 0, and the bioluminescence signal at any
619 *t* will simply decrease by a factor $c_{\mathrm{M}}^{*,\infty} / c_{\mathrm{M}}^{*,0} \sim 1/\left(1 + \varphi / \varphi^*\right)$ (**Figure 3C**) as compared to the signal obtained
620 under non-depletive condition (**Figure 5A**). The bioavailable metal concentration perceived by the
621 biosensor (i.e. $c_{\mathrm{M}}^{*,\infty}$) can then significantly differ from the one prevailing at $t = 0$ (i.e. $c_{\mathrm{M}}^{*,0}$) depending on
622 the magnitude of the ratio φ / φ^*.

In cases where $\tau_{\mathrm{depl}} / \tau_{\mathrm{biol}} \sim 1$ (**Figure 5B**), the second term in Eq. (40) contributes significantly to $Lum(t)$. In turn, for values of φ / φ^* underlying a significant bulk M depletion, the overall dependence of the signal on time differs from the one that holds under non-depletive condition (**Figure 5B**). In detail, while the maximum of the signal decreases with φ / φ^* as a result of decreasing $c_{\mathrm{M}}^{*,\infty} / c_{\mathrm{M}}^{*,0}$, the position $t_{\max}$ marking that maximum is now shifted to lower values with increasing φ / φ^*. This shift is due to the crosstalk between activation kinetics of cell photoactivity ($\sim 1 / \tau_{\mathrm{biol}}$) and M depletion kinetics ($\sim 1 / \tau_{\mathrm{depl}}$), as subsumed in the second term of Eq. (40) (cf. the respective positioning of the blue and red dotted curves in **Figure 5B**, and cf. **Figure S1** in **SI**† for further details). This crosstalk implies that a biosensor will probe at time *t* a larger metal fraction as compared to the situation where $\tau_{\mathrm{depl}} / \tau_{\mathrm{biol}} << 1$. As a result, the extent of decrease in $\overline{Lum}(t) / \overline{Lum}_{\max}\big|_{\varphi << \varphi^*}$ with φ / φ^* will be lower than that pertaining to the situation $\tau_{\mathrm{depl}} / \tau_{\mathrm{biol}} << 1$: this finding is illustrated in **Figure 5C** where $\overline{Lum}_{\max} / \overline{Lum}_{\max}\big|_{\varphi << \varphi^*}$ is plotted versus φ / φ^* in the situations $\tau_{\mathrm{depl}} / \tau_{\mathrm{biol}} << 1$ and $\tau_{\mathrm{depl}} / \tau_{\mathrm{biol}} \sim 1$. Refined analysis of the dependence of $t_{\max}$ on φ / φ^* (**Figure 5D**) indicates that: $t_{\max}$ first decreases with increasing φ / φ^* due to the aforementioned crosstalk between decay of bulk M concentration and increase in cell photoactivity over time, then $t_{\max}$ reaches a minimum and finally increases at sufficiently large φ / φ^* towards the value achieved in the absence of M depletion. The latter increase of $t_{\max}$ with φ / φ^* is explained by the corresponding change in τ_{depl}: the larger is φ / φ^*, the faster the depletion process becomes (cf. Eq. (31) and §2.2), and for $\varphi / \varphi^* >> 1$ bulk M depletion can therefore reach equilibrium before cell photoactivity has significantly increased. Accordingly, at sufficiently high φ / φ^* the overlap between the time windows over which $c_{\mathrm{M}}^*(t)$ decreases and $\overline{c}_{\mathrm{B,p}}(t)$ increases becomes considerably reduced, and $t_{\max}$ then necessarily returns to the values that hold in the absence of M depletion, i.e. for $\varphi / \varphi^* << 1$ (**Figure 5A**). This also explains why the ratios $\overline{Lum}_{\max} / \overline{Lum}_{\max}\big|_{\varphi << \varphi^*}$ evaluated at sufficiently high φ / φ^* under the conditions of **Figures 5A** and **5B** are similar (**Figure 5C**).

Finally, in the trivial situation $\tau_{\mathrm{depl}} / \tau_{\mathrm{biol}} >> 1$, bulk M depletion is so sluggish that cell photoactivity has increased from 0 to 1 well before bulk M depletion started. A biosensor then essentially 'feels' the initial M concentration $c_{\mathrm{M}}^{*,0}$, and the corresponding signal $Lum(t)$ will remain independent of bulk M depletion (i.e. φ / φ^*, **Figures 5C,D**). Last, we mention that the shapes of the signals given for $\varphi / \varphi^* << 1$ in **Figures**

5A and **5B** are different because the transition between $\tau_{depl} / \tau_{biol} << 1$ (**Figure 5A**) to $\tau_{depl} / \tau_{biol} \sim 1$ (**Figure 5B**) is realized here by decreasing the excretion kinetic constant k_e (which slows bulk M depletion down, cf. §2.2.3) while maintaining the value of τ_{biol} identical in **Figures 5A** and **5B**. In turn, the time-dependence of $F(t)$ in Eq. (39) is modified and, therewith, the shape of the signal $Lum(t)$, as detailed elsewhere.[22]

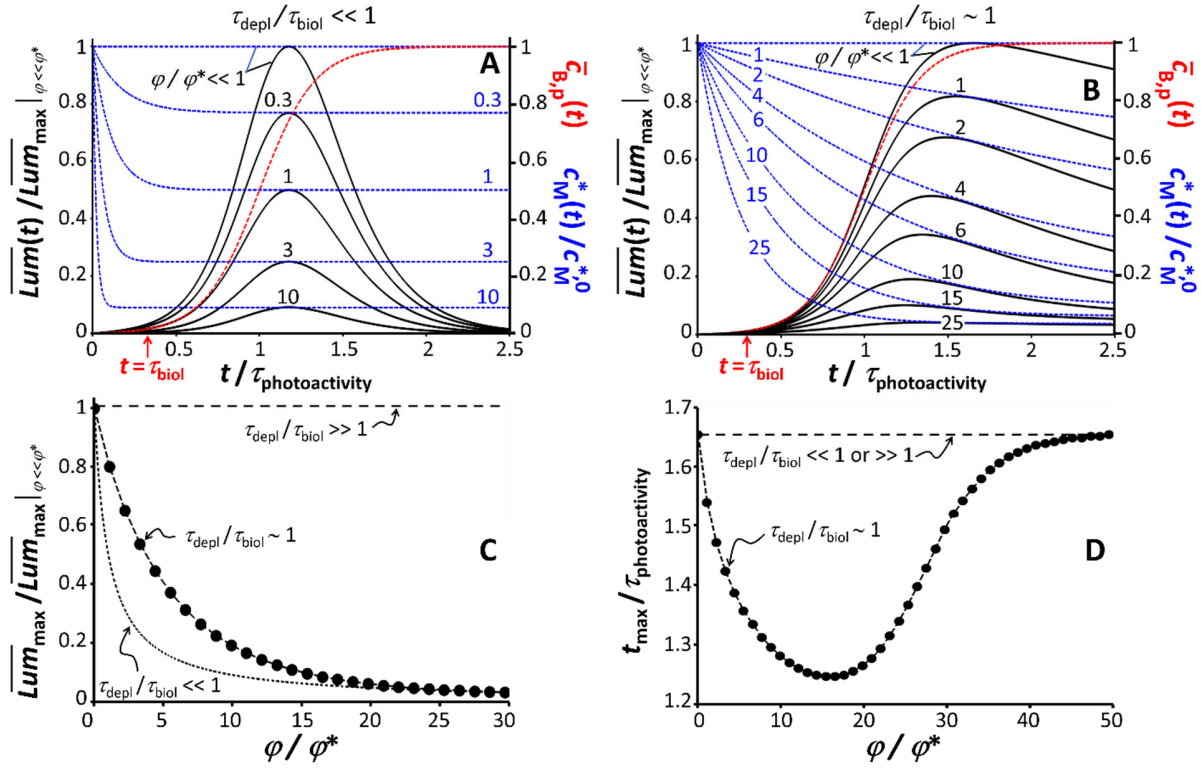

Figure 5. Illustrations of the dependence of the dimensionless bioluminescence signal $\overline{Lum}(t) / \overline{Lum}_{max}\big|_{\varphi<<\varphi^*}$ on time (evaluated from Eq. (39)) for different normalized biosensor concentrations, φ / φ^* (indicated), in the situations $\tau_{depl} / \tau_{biol} << 1$ **(A)** and $\tau_{depl} / \tau_{biol} \sim 1$ **(B).** τ_{depl} is the timescale for depletion of bulk M concentration (it depends on φ / φ^*) and τ_{biol} marks the onset of the increase in the concentration $\overline{c}_{B,p}(t)$ of photoactive cells with time (red dotted curves). The time axis is scaled by $\tau_{photoactivity}$ which is the time at which $\overline{c}_{B,p}(t)$ features an inflexion point. Blue dotted curves represent the time-dependent (dimensionless) bulk M concentration, $c_M^*(t) / c_M^{*,0}$, evaluated for each selected φ / φ^* (Eqs. (14)-(22) or, equivalently, Eq. (25) under the conditions adopted in this figure). The (dimensionless) maxima of bioluminescence signals and their time-positions, $t_{max} / \tau_{photoactivity}$, under the conditions adopted in **(B)** (where $\tau_{depl} / \tau_{biol} \sim 1$) are reported in **(C)** and **(D)**, respectively. We further provide in **(C)** and **(D)** the (dimensionless) signal maxima and associated $t_{max} / \tau_{photoactivity}$, respectively, as a function of φ / φ^* in the extremes $\tau_{depl} / \tau_{biol} << 1$ and $\tau_{depl} / \tau_{biol} >> 1$ (indicated). Unless otherwise specified in the figure, adopted model parameters are: $\overline{K}_{ML} = 10$, $\varepsilon = 1$, $a = 1$ μm, $D_M = 10^{-9}$ m^2 s^{-1}, $Bn^{-1} = 0.1$, $\xi \to 0$, $\overline{K}_i = 10$, $\tau_{a,i} = 0.1$ s, $k_r \tau_{a,i} = 10^{-4}$, $\tau_{photoactivity} = 15$ h, $k_e = 10^{-3}$ s^{-1} **(A)**, $k_e = 10^{-4.5}$ s^{-1}

(B,C,D). The expression adopted for $F(t)$ in Eq. (39) is defined by Eq. (16) in Ref. [22]. In **(C)** and **(D)**, the dotted lines connecting symbols are guides to the eye.

In **Figures 6A,B**, we replot **Figures 5A,B** in the form $Lum(t)/\left(\psi\theta c_{\mathrm{M,t}}^{*,0}\right)$ (in m^{-2}) versus $t/\tau_{\mathrm{photoactivity}}$ in order to investigate how the signal (and its amplitude $Lum_{\max}$) produced by *the ensemble of bacterial sensors* are affected by the ratio φ/φ^{*}, with account of the φ-contributions stemming from ***both*** the convolution product and its prefactor in Eq. (39). Results are first analysed for situations where passive M adsorption on the surface of the biosensors is insignificant, i.e. $\tilde{K}_{\mathrm{H}}=0$ or, equivalently, $\varepsilon_{\mathrm{ads}}=0$ with $\varepsilon_{\mathrm{ads}}$ the (dimensionless) passive adsorption coefficient defined by $\varepsilon_{\mathrm{ads}}=\tilde{K}_{\mathrm{H}}S_{\mathrm{a}}/V_{\mathrm{B}}$.

In the case $\tau_{\mathrm{depl}}/\tau_{\mathrm{biol}}\ll 1$ where the time-position $t_{\max}$ of the bioluminescence peak is independent of φ/φ^{*} (cf. **Figures 5A,D**), an increase in φ/φ^{*} now leads to an increase in $Lum(t)/\left(\psi\theta c_{\mathrm{M,t}}^{*,0}\right)$ (**Figure 6A**), and at any *t* this increase amounts to a factor $Lum_{\max}\big|_{\varphi}/Lum_{\max}\big|_{\varphi\ll\varphi^{*}}\left(>1\right)$ relative to the signal at $\varphi/\varphi^{*}\ll 1$. This modification of the signal contrasts with the one discussed using the representation $\overline{Lum}(t)/\overline{Lum}_{\max}\big|_{\varphi\ll\varphi^{*}}$ selected in **Figure 5A**. This is so because the quantity $Lum(t)/\left(\psi\theta c_{\mathrm{M,t}}^{*,0}\right)$ includes the balance between two opposite effects generated on bioluminescence when increasing cell concentration at $\varepsilon_{\mathrm{ads}}=0$, namely: an increase of bulk M depletion with a resulting decrease of the signal (as specifically analysed in **Figure 5A**), *and* an increase in the number of light-emitting cells with a resulting increase of the bioluminescence, which is the dominant effect in **Figure 6A**. For $\tau_{\mathrm{depl}}/\tau_{\mathrm{biol}}\ll 1$, it is easily shown from Eq. (39) that $Lum_{\max}$ scales with φ according to

$$Lum_{\max}\sim\varphi\left(1-\varepsilon_{\mathrm{ads}}\varphi\right)/\left(1+\varphi/\varphi^{*}\right) \tag{41}$$

Equation (41) makes it transparent that linearity between $Lum_{\max}$ and φ is conserved on the premise that $\varphi/\varphi^{*}\ll 1$ and $\varepsilon_{\mathrm{ads}}\varphi\ll 1$. Eq. (41) further conforms to the $Lum_{\max}/\left(\psi\theta c_{\mathrm{M,t}}^{*,0}\right)$ data provided in **Figure 6C** for $\varepsilon_{\mathrm{ads}}=0$, with a linear increase of $Lum_{\max}/\left(\psi\theta c_{\mathrm{M,t}}^{*,0}\right)$ when increasing φ/φ^{*} in the range $\varphi/\varphi^{*}\ll 1$, and a plateau value (proportional to φ^{*}) reached at $\varphi/\varphi^{*}\gg 1$. The denominator and numerator in Eq. (41) taken in the limit $\varepsilon_{\mathrm{ads}}\varphi\ll 1$ capture the balance between the two opposite effects induced on the signal when increasing cell volume fraction. This balance is obviously modified by M passive adsorption, which is evidenced in **Figure 6C** where $Lum_{\max}/\left(\psi\theta c_{\mathrm{M,t}}^{*,0}\right)$ is reported as a function of φ/φ^{*} for increasing values of $\varepsilon_{\mathrm{ads}}$. In agreement with Eq. (41), **Figure 6C** shows the quadratic dependence of $Lum_{\max}$ on φ/φ^{*}

for $\varphi / \varphi^* << 1$ and sufficiently high ε_{ads}, and a linear decrease of $Lum_{\max}$ with increasing φ at $\varphi / \varphi^* >> 1$ (with slope $-\varepsilon_{\text{ads}} \varphi^*$).

For the situation $\tau_{\text{depl}} / \tau_{\text{biol}} \sim 1$ (**Figure 6B**), the signal $Lum(t) / \left(\psi \theta c_{\text{M,t}}^{*,0} \right)$ is characterised by a shift of the position $t_{\max}$ of the maxima with varying φ / φ^* (as explained in **Figure 5D**) and by a non-monotonous variation of the signal maxima with increasing φ / φ^* (cf. black and coloured curves in **Figure 6B**). In detail, for $\varepsilon_{\text{ads}} = 0$, $Lum_{\max}$ increases with φ / φ^*, reaches a maximum, decreases before slightly increasing to finally reach a constant plateau value at $\varphi / \varphi^* >> 1$ (**Figure 6D)**. The existence of such a maximum in the representation $Lum_{\max}$ versus φ / φ^* is -together with the companion dependence of $t_{\max}$ on φ / φ^* (**Figure 5D**)- the signature of the significant crosstalk discussed in **Figure 5** between activation kinetics of cell photoactivity and M depletion kinetics for $\tau_{\text{depl}} / \tau_{\text{biol}} \sim 1$. This crosstalk allows indeed cells to 'feel' a larger bioavailable M fraction as compared to the situation where M depletion would be completed well before $\overline{c}_{\text{B,p}}(t)$ starts to increase over time. At sufficiently large φ / φ^*, τ_{depl} becomes lower than τ_{biol}, and the bulk M concentration probed by the biosensors then gradually reduces to $c_{\text{M}}^{*,\infty} / c_{\text{M}}^{*,0} \approx 1 / \left(1 + \varphi / \varphi^* \right)$ so that $Lum_{\max}$ then reaches the plateau value that would hold in the absence of M passive adsorption, in agreement with **Figure 6D** and Eq. (41) taken in the limit $\varphi / \varphi^* >> 1$. The slight increase of $Lum_{\max}$ with φ / φ^* (observed under the selected conditions) that just precedes the achievement of that plateau is simply due to the increase of light-emitting cells (factor φ in the numerator of Eq. (41)). The introduction of M passive adsorption decreases the maximum identified in the plot $Lum_{\max}$ versus φ / φ^* at $\varepsilon_{\text{ads}} = 0$ (**Figure 6D**), and it leads to a linear decrease of $Lum_{\max}$ versus φ / φ^* at $\varphi / \varphi^* >> 1$ with a slope $-\varepsilon_{\text{ads}} \varphi^*$, similarly to the trend discussed in **Figure 6C** for $\tau_{\text{depl}} / \tau_{\text{biol}} << 1$.

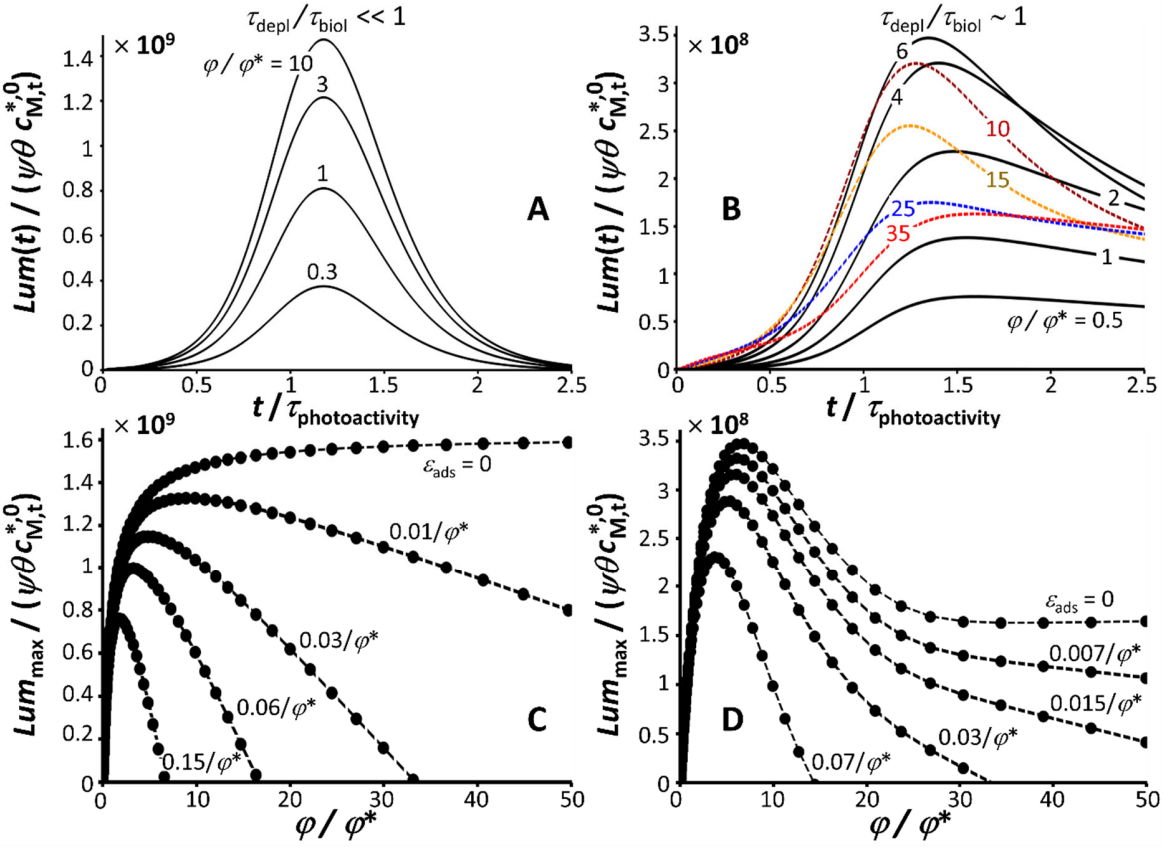

Figure 6. **(A,B)** As in Figure 5A and 5B, except that bioluminescence signals are reported in the form $Lum(t)/\left(\psi\theta c^{*,0}_{M,t}\right)$ for selected values of φ/φ^* (indicated). Model parameters in **(A)** and **(B)**: as in Figure 5A and 5B, respectively, with $\varepsilon_{ads}=0$. Bioluminescence maxima under the conditions holding in **(A)** and **(B)** are collected as a function of φ/φ^* in **(C)** and **(D)**, respectively. The way the dependence of these maxima on φ/φ^* is affected by passive adsorption of M at the surface of the biosensors is further illustrated in **(C)** and **(D)** where computations are given for different ε_{ads} (indicated). In **(C)** and **(D)**, dotted lines are guides to the eye. Coloured lines in **(B)** mark non-monotonous variations of $Lum(t)/\left(\psi\theta c^{*,0}_{M,t}\right)$ with changing φ/φ^*.

3.3. Effects of ligand concentration on the bioluminescence signal $Lum(t)$.

In practice, the options for tuning the bioluminescence response so as to address metal bioavailability properties are not limited to varying cell concentration but also include the possibility to change the concentration c^*_L of ligand in solution: this comes to modify the value of the dimensionless ML stability constant, $\bar{K}_{ML}=K_{ML}c^*_L$. Accordingly, we report in **SI**† (**Figure S2)** and **Figures 7A,B** the analogues of **Figure 5** and **Figures 6A,B** with bioluminescence signals that are computed for increasing values of $\bar{K}_{ML}$ at fixed value of φ and $\varepsilon_{ads}=0$. To ease interpretation, simulations of $Lum(t)/\left(\psi\theta c^{*,0}_{M,t}\right)$ in **Figures 7A,B** are given

for ML lability $\xi \to 0$, which ensures that the function $F(t)$ (and k_{eff}, cf. Eq. (38)) involved in Eq. (39) remains unchanged with varying $\bar{K}_{\text{ML}}$. Briefly, for both cases $\tau_{\text{depl}} / \tau_{\text{biol}} << 1$ (**Figure 7A**) and $\tau_{\text{depl}} / \tau_{\text{biol}} \sim 1$ (**Figure 7B**), the observed modifications of the bioluminescence response with *increasing* $\bar{K}_{\text{ML}}$ at given φ are qualitatively similar to those discussed in **Figures 6A** and **6B** when *decreasing* φ / φ^* at fixed $\bar{K}_{\text{ML}}$, and the same conclusion holds for the signals produced by a single metal-sensing cell (**Figure S2** to be compared with **Figure 5**). We observe: (i) a monotonous and non-monotonous decrease of $Lum_{\max} / \left(\psi \theta c_{\text{M,t}}^{*,0} \right)$ with increasing $\bar{K}_{\text{ML}}$ for $\tau_{\text{depl}} / \tau_{\text{biol}} << 1$ (**Figures 7A,C**) and $\tau_{\text{depl}} / \tau_{\text{biol}} \sim 1$ (**Figures 7B,D**), respectively, with the apparition of a shallow maximum for $Lum_{\max} / \left(\psi \theta c_{\text{M,t}}^{*,0} \right)$ versus $\bar{K}_{\text{ML}}$ in the latter situation (**Figure 7D**), and (ii) the absence and presence of a dependence of $t_{\max}$ on $\bar{K}_{\text{ML}}$ for $\tau_{\text{depl}} / \tau_{\text{biol}} << 1$ and $\tau_{\text{depl}} / \tau_{\text{biol}} \sim 1$ (cf. inset **Figure 7B**), respectively. The decrease of $Lum_{\max} / \left(\psi \theta c_{\text{M,t}}^{*,0} \right)$ at sufficiently high $\bar{K}_{\text{ML}}$ for $\tau_{\text{depl}} / \tau_{\text{biol}} << 1$ is the result of the decrease in the initial free M concentration, $c_{\text{M}}^{*,0}$, according to $c_{\text{M}}^{*,0} = c_{\text{M,t}}^{*,0} / \left(1 + \bar{K}_{\text{ML}} \right)$ (cf. Eq. (39)). This effect of $\bar{K}_{\text{ML}}$ dominates the increase in bioluminescence that would be observed as a result of the only ligand-mediated buffering of M depletion illustrated in **Figure 4** (cf. **Figure S2A**). For $\tau_{\text{depl}} / \tau_{\text{biol}} \sim 1$, features (i) and (ii) above are again the results of the interplay between M depletion kinetics and activation kinetics of cell photoactivity. In detail, under the conditions selected in **Figure 7B**, $t_{\max}$ increases with $\bar{K}_{\text{ML}}$ according to a sigmoid-like dependence, and it reaches a plateau value at $\bar{K}_{\text{ML}} >> 1$ (inset **Figure 7B**). The evolution of $t_{\max}$ with increasing $\bar{K}_{\text{ML}}$ from values <<1 to >>1 is qualitatively identical to that produced when decreasing φ from >>1 to <<1 because $\bar{K}_{\text{ML}}$ and φ acts on depletion kinetics (and thus on the extent of crosstalk between depletion and cell photoactivity) in opposite ways: increasing φ fastens depletion (cf. blue dotted curves in **Figures 5A,B**) whereas increasing $\bar{K}_{\text{ML}}$ slows depletion down (**Figure 4A** and **Figure S2B**). This argument also explains, qualitatively, the mirror evolutions of $Lum_{\max}$ with $\bar{K}_{\text{ML}}$ and φ in **Figure 7D** and **Figure 6D**, respectively. Depending on the respective magnitudes of $\tau_{\text{photoactivity}}$ (and therewith τ_{biol}) and τ_{depl}, a local minimum in the dependence of $t_{\max}$ on $\bar{K}_{\text{ML}}$ may further exist (**Figure S2D**). This minimum is the pendant of the one observed in **Figure 5D** when varying φ / φ^* at fixed $\bar{K}_{\text{ML}}$. Quantitatively, from Eq. (39) taken in the limit $\xi \to 0$ and $\tau_{\text{depl}} / \tau_{\text{biol}} << 1$, we infer the following scaling of $Lum_{\max}$ with $\bar{K}_{\text{ML}}$

$$Lum_{\max} \sim \varphi \left(1 - \varepsilon_{\text{ads}} \varphi \right) / \left[\left(1 + \varphi / \varphi^* \right) \left(1 + \bar{K}_{\text{ML}} \right) \right] \tag{42}$$

where the expression of φ^* *involves* $\bar{K}_{\mathrm{ML}}$ according to Eq. (32). In agreement with Eq. (42), for the regime $\bar{K}_{\mathrm{ML}} >> 1$ where buffering of bulk M concentration by L is very efficient and M depletion becomes insignificant, $\mathrm{Log}\left(Lum_{\max}\right)$ then decreases with slope -1 with increasing $\mathrm{Log}\left(\bar{K}_{\mathrm{ML}}\right)$ (**Figures 7C,D**). For illustration, the dependence of $Lum_{\max} / \left(\psi\theta c_{\mathrm{M,t}}^{*,0}\right)$ on $\bar{K}_{\mathrm{ML}}$ is shown in linear scale for $\varepsilon_{\mathrm{ads}} = 0$ in the insets of **Figures 7C,D**. At fixed $\bar{K}_{\mathrm{ML}}$ and φ, M passive adsorption reduces $Lum_{\max}$ (**Figures 7C,D**), in agreement with Eq. (42). Interestingly, combining Eqs. (32) and (42) in the limits $\varphi / \varphi^* >> 1$ and $\varepsilon_{\mathrm{ads}}\varphi << 1$ leads to

$$Lum_{\max} \sim \frac{a^2 k_{\mathrm{e}}}{3 D_{\mathrm{M}} Bn^{-1}} \frac{1}{1+\bar{K}_{\mathrm{i}}} \tag{43}$$

, which is independent of extracellular metal speciation conditions and biosensor concentration in solution.

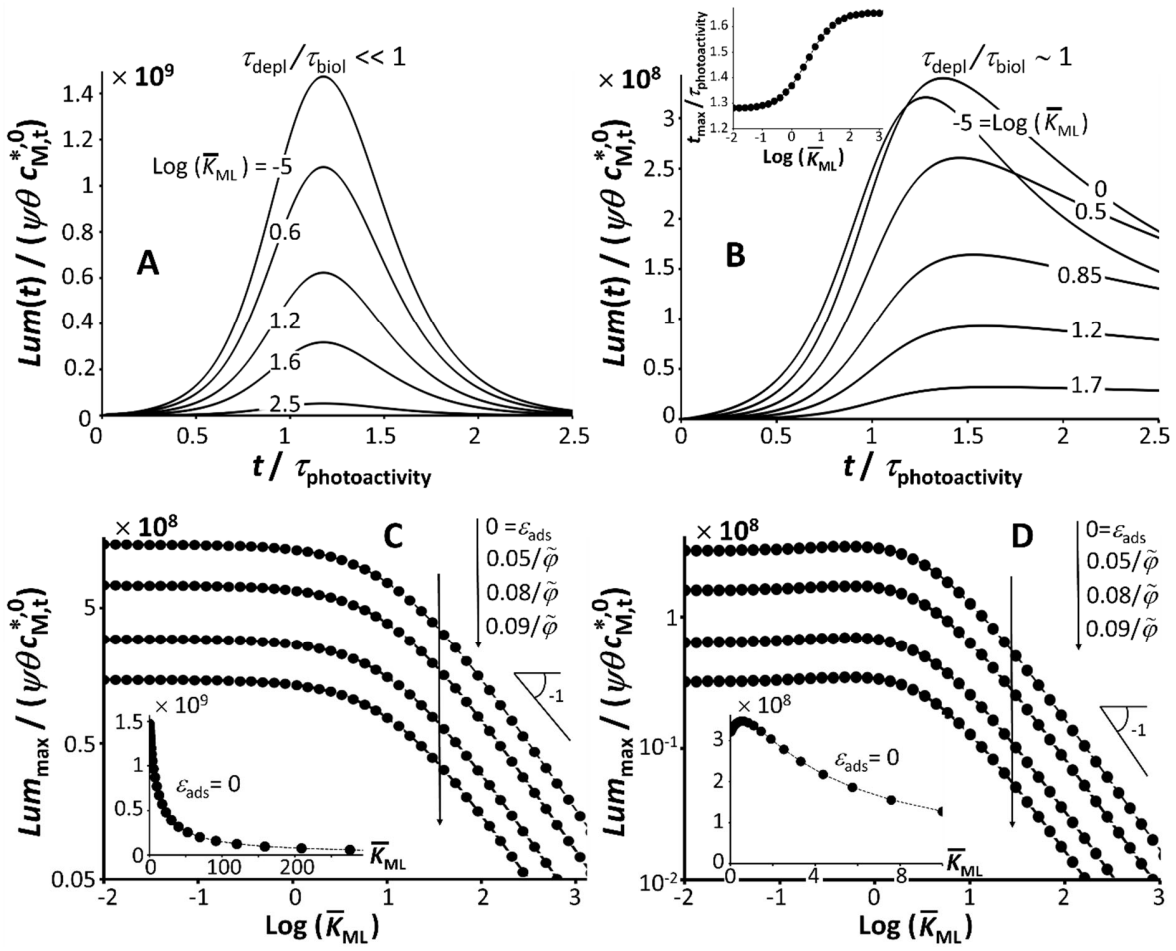

Figure 7. Panels **(A)**, **(B)**, **(C)** and **(D)** are the analogues of Figures 6A, 6B, 6C, 6D, respectively, with the focus given here on biosensor's time-response evaluated for selected values of $\bar{K}_{\mathrm{ML}}$ (indicated) at constant cell volume

fraction $\varphi / \tilde{\varphi} = 10$ with $\tilde{\varphi}$ defined by $\tilde{\varphi} = \varphi^* / \left(1 + \bar{K}_{\mathrm{ML}}\right)$ which is independent of $\bar{K}_{\mathrm{ML}}$ (cf. the definition of φ^* by Eq. (32)). Other model parameters in **(A)**,**(C)** and **(B)**,**(D)**: as in Figures 6A,C and 6B,D, respectively. Inset panel **(B)**: time-position $t_{\max} / \tau_{\mathrm{photoactivity}}$ of the bioluminescence maxima versus Log($\bar{K}_{\mathrm{ML}}$) under the conditions that hold in **(B)**. Insets panels **(C)** and **(D)**: representation of the bioluminescence maxima for $\varepsilon_{\mathrm{ads}} = 0$ according to linear scale in $\bar{K}_{\mathrm{ML}}$. In **(B)-(D)**, symbols are computed data and dotted lines are guides to the eye.

Finally, we recall that $c_{\mathrm{M}}^{*,\infty} / c_{\mathrm{M}}^{*,0}$ and τ_{depl} depend on the bioavailability features of M *and* ML species (cf. **Table 1** and **Figures 2-4**), i.e. on Bn^{-1} and ML lability ξ . Accordingly, changes in the amplitude and apparition delay of bioluminescence maxima and/or modification of signal shape with increasing φ and/or $\bar{K}_{\mathrm{ML}}$ (**Figures 5-7**) at given $\bar{c}_{\mathrm{B,p}}(t)$ can be viewed as intrinsic markers of the nature of the M biouptake flux (i.e. internalized- or diffusion-controlled), of ML inertness and -if applicable- ML lability (**Figure 2**). Observed change in the time response of the biosensors measured with varying φ , c_{L}^* and/or nature of L, thus necessarily reflect the dependence of M biouptake flux and M depletion on Bn^{-1} and ξ (cf. discussion in §2.2.3-2.2.4), and/or the way in which $F(t)$ varies with k_{eff} which is also function of Bn^{-1} and ξ (cf. below Eq. (38)). For the latter aspect, the reader is referred to our previous work[22] where we detailed how the shape of the bioluminescence signal is modulated by k_{eff} and by the dependence of cell photoactivity on time. The theory thus highlights here the benefits of systematic measurements of the time-response of luminescent biosensors as a function of *both* ligand and cell concentrations in solution in order to extract relevant information on M speciation properties and bioaccumulation kinetic features from cell signal analysis. In a coming contribution, the remarkable properties of bioluminescence signal produced by metal biosensors -as evidenced here by theory- will be supported by experiments on Cd-sensing *luxCDABE-Escherichia* in various metal-complexing medium conditions. Based on the theory and the defining expression of bioluminescence signal detailed here, a proper signal normalization and time-deconvolution procedure will be elaborated to *analyze quantitatively the full biosensor response measured over time* and therewith evaluate relevant metal bioavailability and bioaccumulation kinetic properties.

4. Conclusions and perspectives.

In this work, we elaborate an original and comprehensive theory that details how the time-response of metal *lux*-bacterial sensors is determined by the dynamic partitioning of bioactive (free) metal species at the interface between biosensor and aqueous medium. This partitioning is tackled by a mechanistic formulation of the coupling between kinetics of bulk metal depletion, chemodynamics of intracellular

771 metal complexes formed with the regulatory protein of the metal bioreporter, and dynamics of the
772 reactive transfer of metal species from solution to the metal-accumulating interface. Reasoning beyond
773 the equilibrium hypothesis underlying the applicability of standard BLM modeling, this metal reactive
774 transfer involves here the interplay between steady-state diffusion of free and complexed metal species,
775 the kinetics of formation/dissociation of metal complexes formed with metal-binding ligands in solution,
776 and the kinetics of metal bioaccumulation and excretion. In turn, an explicit expression is developed for
777 the bioluminescence signal produced by metal *lux*-biosensors as a function of biosensor and metal ligand
778 concentrations in solution, and the key biophysicochemical determinants of intra/extracellular metal
779 speciations, metal depletion kinetics and metal bioavailability. The formalism allows identification of the
780 scenarios where metal biouptake is rate-limited by metal internationalization (applicable in BLM) or
781 diffusion, and the cases where metal complexes in solution are inert, dynamic, non-labile or fully labile
782 depending on their contribution to the biouptake flux of free metal. On the basis of a set of computational
783 examples, we then discuss how time-dependent signals generated by metal biosensors are modified with
784 varying concentration of metal-sensing cells and extracellular metal-binding ligands. In particular, we
785 explain why the crosstalk between kinetics of bulk metal depletion (which is speciation-dependent) and
786 activation kinetics of cell photoactivity (connected to cell metabolism and quality/quantity of nutrients)
787 can generate shifts in the delay of apparition of bioluminescence maxima, and a non-monotonous
788 dependence of these maxima on cell concentration and concentration/strength of ligands in solution.

789 Overall, the conceptual framework detailed here paves the way for a promising processes-based
790 interpretation/exploitation of metal bioreporter response over time and the evaluation of metal
791 bioavailability features beyond restrictive BLM foundation, i.e. with account of intertwined dynamics of
792 extracellular *and* intracellular mechanisms that contribute to metal-triggered bioluminescence emission.
793 Obviously, extensions of the theory will be required to treat metal speciation conditions more involved
794 than those considered here for demonstration purpose, especially for cases where e.g.: (i) metal
795 speciation in solution is significantly controlled by different types of ligands, (ii) bioactive metal forms
796 include complexed metal species, or (iii) there is competition between metal species probed by the
797 biosensors and other ionic solution components for occupancy of the internalisation sites at the biosensor
798 surface.[43,44] The theoretical scheme detailed in this work constitutes a starting basis for such future
799 extensions. Last, we stress that the findings derived here also apply to cell signals featuring successive
800 bioluminescence peaks over time.[21,23] The extent to which the positioning and amplitude of a given peak
801 is impacted by changes of biosensor and ligand concentrations will indeed depend on how fast metal

depletion in solution operates as compared to the time-increase of cell photoactivity corresponding to the mode of bioluminescence emission[21] at the origin of that peak.

Glossary of main abbreviations and symbols.

Abbreviations

BLM Biotic Ligand Model

L Metal-binding ligand in solution

M Free (not complexed) metal (the only bioaccumulated metal form in this work)

ML Metal complex formed between M and L in solution

MP_{reg} Intracellular complex formed between M and P_{reg}

P_{reg} Metal-binding regulatory protein

Latin

a Radius of the biosensor (m)

Bn^{-1} Reciprocal of the Bosma number Bn defined by Eq. (20)

c_{B} Number concentration of biosensors in solution (includes both photoactive and photoinactive cells) (m^{-3})

$c_{\mathrm{B,p}}^{\max} = \theta c_{\mathrm{B}}$ Maximum number concentration of photoactive cells the medium can sustain depending on available nutrients therein (m^{-3}), with $0 < \theta \leq 1$

c_{L}^{*} Bulk solution concentration of ligand L (mol m^{-3})

$c_{\mathrm{M}}^{*,0}$ Bulk solution concentration of free metal M at $t = 0$ (mol m^{-3})

$c_{\mathrm{M,t}}^{*,0}$ Total bulk concentration of metal species at $t = 0$ (mol m^{-3})

$c_{\mathrm{M}}^{*,\infty}$ Bulk concentration of free metal M at equilibrium ($t \to \infty$) (mol m^{-3})

$c_{i=\mathrm{M,L,ML}}\left(r,t\right)$ Concentrations of M, L, ML species at position r and time t (mol m^{-3})

$c_{i=\mathrm{M,ML}}^{*}\left(t\right)$ Bulk concentrations of M and ML at time *t* (mol m^{-3})

$\overline{c}_{i=\mathrm{M,ML}}\left(r,t\right)$ Dimensionless concentrations of M and ML at position r and time *t* defined by $\dfrac{c_{i=\mathrm{M,ML}}\left(r,t\right)}{c_{i=\mathrm{M,ML}}^{*}\left(t\right)}$

$\overline{c}_{\mathrm{B,p}}\left(t\right)$ Dimensionless concentration of photoactive cells at time *t*

$c_{\mathrm{M}}^{a}\left(t\right)$ Surface concentration of free M at time *t* (mol m^{-3})

$D_{i=\mathrm{M,L,ML}}$ Diffusion coefficients of M, L and ML in solution ($m^2\ s^{-1}$)

$f_{\mathrm{a,M}}$ Dimensionless scalar defined by Eq. (21)

$F\left(t\right)$ Dimensionless function involved in the convolution product of Eqs. (37),(39)

$J_{\mathrm{e}}\left(t\right)$ M excretion flux at time *t* (mol $m^{-2}\ s^{-1}$)

$J_{\mathrm{u}}\left(t\right)$ M biouptake flux at time *t* (mol $m^{-2}\ s^{-1}$)

$J_{\mathrm{M}}\left(t\right)$ Supply flux of M at time *t* (mol $m^{-2}\ s^{-1}$)

k_{a} , k_{d} Kinetic constants for ML formation ($m^3\ mol^{-1}\ s^{-1}$) and dissociation (s^{-1}) in solution, respectively

$k_{\mathrm{a,i}}^{*}$, $k_{\mathrm{d,i}}^{*}$ Kinetic constants for intracellular MP_{reg} formation ($m^3\ mol^{-1}\ s^{-1}$) and dissociation (s^{-1}), respectively

k_{e} Kinetic constant for M excretion (s^{-1})

k_{eff} Effective kinetic constant defined below Eq. (38) (s^{-1})

k_{int} Internalization kinetic constant (s^{-1})

k_{r} Effective kinetic constant associated with the inhibition of luciferase production and/or activity (s^{-1})

841 K_{H} Henry constant for adsorption of M on the internalisation sites at the biosensor surface (m)

842 $\tilde{K}_{\mathrm{H}}$ Henry constant for passive adsorption of M at the biosensor surface (m)

843 K_{Hi} Hill constant that relates to the affinity of the promoter for the MP_{reg} complex (mol m^{-3})

844 $\overline{K}_{\mathrm{i}} = \tau_{\mathrm{d,i}} / \tau_{\mathrm{a,i}}$ Dimensionless stability constant for intracellular MP_{reg} complex

845 K_{ML} ML stability constant (m^3 mol^{-1})

846 $\overline{K}_{\mathrm{ML}}$ Dimensionless ML stability constant defined by $\overline{K}_{\mathrm{ML}} = K_{\mathrm{ML}} c_{\mathrm{L}}^{*}$

847 $Lum^{(0)}(t,x,y)$ Bioluminescence (counts s^{-1}) at time *t* in the absence of bulk M depletion under conditions where
848 bulk M concentration is *x* and (time-dependent) cell photoactivity is *y* (Eq. (37))

849 $Lum(t)$ Bioluminescence at time *t* with account of bulk M depletion (counts s^{-1}) (Eq. (39))

850 $Lum_{\max}$ Maximum of the time-dependent bioluminescence signal $Lum(t)$ (counts s^{-1})

851 $\overline{Lum}(t)$ Bioluminescence (counts s^{-1} m^3) at time *t* defined by $Lum(t) / \left[c_{\mathrm{B}} \left(1 - \tilde{K}_{\mathrm{H}} S_{\mathrm{a}} c_{\mathrm{B}} \right) \right]$

852 $\overline{Lum}_{\max} / \overline{Lum}_{\max}\Big|_{\varphi << \varphi^{*}}$ Dimensionless ratio between maxima of $\overline{Lum}(t)$ evaluated with and without account of
853 bulk M depletion

854 p_{ML} Dimensionless scalar defined by $p_{\mathrm{ML}} = p_{\mathrm{o}} / \left(1 - \varphi^{1/3} \right)$

855 p_{o} Dimensionless scalar defined by $p_{\mathrm{o}} = 1 + \varepsilon \overline{K}_{\mathrm{ML}} \xi$

856 r_{c} Radius of Kuwabara cell defined by $r_{\mathrm{c}} = a \varphi^{-1/3}$

857 S_{a} Surface area of a biosensor (m^2)

858 t Time (s)

859 $\overline{t} = t / \tau_{\mathrm{a,i}}$ Dimensionless time after scaling of *t* by $\tau_{\mathrm{a,i}}$

860 V_{B} Volume of a biosensor (m^3)

861

862 ***Greek***

863 ε Ratio defined by $\varepsilon = D_{\mathrm{ML}} / D_{\mathrm{M}}$

864 $\varepsilon_{\mathrm{ads}}$ Dimensionless number for passive adsorption of M at the biosensor surface defined by $\varepsilon_{\mathrm{ads}} = \tilde{K}_{\mathrm{H}} S_{\mathrm{a}} / V_{\mathrm{B}}$

865 ζ Dimensionless scalar defined by Eq. (18)

866 $\overline{\kappa}_{\mathrm{a}}$ (Dimensionless) Damköhler number for the rate constant of ML formation, defined by $\overline{\kappa}_{\mathrm{a}} = k_{\mathrm{a}} c_{\mathrm{L}}^{*} a^2 / D_{\mathrm{M}}$

867 λ_{o} Dimensionless scalar defined by Eq. (19)

868 μ_{o} Reaction layer thickness defined by $\mu_{\mathrm{o}} = \sqrt{D_{\mathrm{M}} / \left(k_{\mathrm{a}} c_{\mathrm{L}}^{*} \right)}$ (m)

869 ξ ML lability parameter defined by Eq. (6) (no dimension)

870 ρ_{s} Concentration of metal-binding sites carried by P_{reg} and smeared-out over the volume of a biosensor (mol m^{-3})

871 $\tau_{\mathrm{a,i}}$ Time constant for the formation of intracellular MP_{reg}, defined by $\tau_{\mathrm{a,i}} = 1 / \left(k_{\mathrm{a,i}}^{*} \rho_{\mathrm{s}} \right)$ (s)

872 $\tau_{\mathrm{d,i}}$ Time constant for the dissociation of intracellular MP_{reg}, defined by $\tau_{\mathrm{d,i}} = 1 / k_{\mathrm{d,i}}^{*}$ (s)

873 τ_{biol} Timescale marking the onset of increase of $\overline{c}_{\mathrm{B,p}}(t)$ with time (s)

874 τ_{depl} Time constant for bulk depletion of M (s) for cases where $c_{\mathrm{M}}^{*}(t)$ decreases with *t* according to a mono-
875 exponential law (Eq. (25))

876 τ_{o} Timescale for transferring M from bulk solution to the intracellular cell volume prior to intracellular sequestration
877 of M by P_{reg} (s)

878 $\overline{\tau}_{\mathrm{o}}$ Dimensionless timescale defined by $\overline{\tau}_{\mathrm{o}} = \tau_{\mathrm{o}} / \tau_{\mathrm{a,i}}$

879 $\tau_{\mathrm{photoactivity}}$ Time at which $\overline{c}_{\mathrm{B,p}}(t)$ features an inflexion point (s)

τ_{SS} Timescale for steady-state M diffusion from solution to biosensor surface defined by $\tau_{SS} = a^2 / D_M$ (s)

$\tau_{\pm} = \tau_{a,i}\bar{\omega}_{\pm}^{-1}$ Time constants for bulk M depletion referring to the short- and long-term depletion components (τ_+ and τ_-, respectively) (Eq. (14))

φ Biosensor volume fraction related to c_B by $\varphi = c_B V_B$

φ^* Critical cell volume fraction defined by Eq. (32)

$\tilde{\varphi}$ Defined by $\tilde{\varphi} = \varphi^* / \left(1 + \bar{K}_{ML}\right)$

$\phi_c(t)$ Concentration of intracellular metal complex MP_{reg} at time *t* per microorganism surface area (mol m^{-2})

$\phi_M(t)$ Concentration of intracellular free M at time *t* per microorganism surface area (mol m^{-2})

ψ Parameter involved in the defining expression of the time-dependent bioluminescence signal (Eqs. (37),(39)) (counts s^{-1} mol^{-1} m^5)

$\bar{\omega}_{\pm}$ Dimensionless frequencies associated to the short- and long-term kinetics of bulk M depletion (Eq. (16))

Data availability

The data that support the findings of this study are available from the corresponding author upon reasonable request.

Conflicts of interest

There are no conflicts of interest to declare.

Acknowledgements

J.F.L.D. is grateful to French national EC2CO program and OTELo (Observatoire Terre Environnement Lorraine) for financial support: Programs EC2CO MENABIOL and AAP Interdisciplinaire OTELo 2020. J.F.L.D. is grateful to Lorraine Université d'Excellence LUE (Program BioCEL) for funding the PhD thesis of L.M.

† Supplementary Information (SI) available

Full expression (Eq. (S1)) of the (dimensionless) quantity $f_{a,M}$ involved in Eqs. (17) and (19), and for which the limit at $\varphi << 1$ leads to Eq. (21). Defining expressions for the concentrations of intracellular free metal $\phi_M(t)$ (Eq. (S2)), intracellular MP_{reg} complex $\phi_c(t)$ (Eq. (S3)) and for the equilibrium concentration of free metal at the surface of a biosensor, $c_M^a(t \to \infty) = c_M^{a,\infty}$ (Eq. (S5)). Supplementary figure (Figure S1) illustrating how bulk metal depletion modifies bioluminescence signal, using the expression that decomposes the signal into the two components defined by Eq. (40). Supplementary figure (Figure S2) reporting the analogue of Figure 5 for analysing the variations of the dimensionless bioluminescence signal $\overline{Lum}(t) / \overline{Lum}_{max}\Big|_{\varphi << \varphi^*}$ as a function of the dimensionless stability constant $\bar{K}_{ML}$ of extracellular ML complex.

References.

[1] A. Tessier, R. Turner, (1995) Metal Speciation and Bioavailability in Aquatic Systems, IUPAC Series on Analytical Chemistry of Environmental Systems. John Wiley and Sons.

[2] H. E. Allen, R. H. Hall, T. D. Brisbin. Metal speciation. Effects on aquatic toxicity. *Environ. Sci. Technol.*, 1980, **14**, 441-443.

[3] C. J. Milne, D. G. Kinniburgh, W. H. van Riemsdijk, E. Tipping. Generic NICA-Donnan model parameters for metal-ion binding by humic substances. *Environ. Sci. Technol.*, 2003, **37**, 958-971.

[4] E. Tipping. WHAMC-A chemical equilibrium model and computer code for waters, sediments, and soils incorporating a discrete site/electrostatic model of ion-binding by humic substances. *Computers & Geosciences*, 1994, **20**, 973-1023.

[5] R. M. Town, van H. P. Leeuwen, J. F. L. Duval. Rigorous physicochemical framework for metal ion binding by aqueous nanoparticulate humic substances: implications for speciation modeling by the NICA-Donnan and WHAM codes. *Environ. Sci. Technol.*, 2019, **53**, 8516-8532.
[6] https://vminteq.com/
[7] S. Niyogi, C. M. Wood. Biotic Ligand Model, a Flexible Tool for Developing Site-Specific Water Quality Guidelines for Metals. *Environ. Sci. Technol.,* 2004, **38**, 23, 6177-6192.
[8] V. Slaveykova, K. Wilkinson. Predicting the bioavailability of metals and metal complexes: Critical review of the biotic ligand model. *Environ. Chem.,* 2005, **2**, 9-24.
[9] H. P. van Leeuwen, R. M. Town, J. Buffle, R. F. M. J. Cleven, W. Davison, J. Puy, W. H. van Riemsdijk, L. Sigg. Dynamic speciation analysis and bioavailability of metals in aquatic systems. *Environ. Sci. Technol.,* 2005, **39**, 22, 8545-8556.
[10] K. J. Wilkinson and J. Buffle, in Physicochemical kinetics and transport at biointerfaces, ed. H. P. van Leeuwen and W. Köster, John Wiley & Sons, Chichester, 2004, chapter 10, p. 445.
[11] H. P. van Leeuwen, Metal speciation dynamics and bioavailability: inert and labile complexes. *Environ. Sci. Technol.* 1999, **33**, 3743-3748.
[12] J. F. L. Duval, E. Rotureau. Dynamics of metal uptake by charged soft biointerphases: impacts of depletion, internalisation, adsorption and excretion. *Phys. Chem. Chem. Phys.*, 2014, **16**, 7401-7416.
[13] J. F. L. Duval, H. P. van Leeuwen, R. M. Town. Electrostatic effects on ligand-assisted transfer of metals to (bio)accumulating interfaces and metal complexes (bioavai)lability. *Colloids Surf. A: Physicochem. Eng. Asp.,* 2023, **658**, 130679.
[14] H. P. van Leeuwen, J. F. L. Duval, J. P. Pinheiro, R. Blust, R. M. Town. Chemodynamics and bioavailability of metal ion complexes with nanoparticles in aqueous media. *Environ. Sci.: Nano.,* 2017, **4**, 2108-2133.
[15] J. P. Pinheiro, J. Galceran, H. P. van Leeuwen. Metal speciation dynamics and bioavailability: bulk depletion effects. *Environ. Sci. Technol.,* 2004, **38**, 2397-2405.
[16] E. Rotureau, P. Billard, J. F. L. Duval. Evaluation of metal biouptake from the analysis of bulk metal depletion kinetics at various cell concentrations: theory and application. *Environ. Sci. Technol.,* 2015, **49**, 990-998.
[17] J. F. L. Duval. Dynamics of metal uptake by charged biointerphases: bioavailability and bulk depletion. *Phys. Chem. Chem. Phys.*, 2013, **15**, 7873-7888.
[18] R. M. Présent, E. Rotureau, P. Billard, C. Pagnout, B. Sohm, J. Flayac, R. Gley, J. P. Pinheiro, J. F. L. Duval. Impact of intracellular metallothionein on metal biouptake and partitioning dynamics at bacterial interfaces. *Phys. Chem. Chem. Phys.*, 2017, **19**, 29114-29124.
[19] J. F. L. Duval, R. M. Présent, E. Rotureau. Kinetic and thermodynamic determinants of trace metal partitioning at biointerphases: the role of intracellular speciation dynamics. *Phys. Chem. Chem. Phys.*, 2016, **18**, 30415-30435.
[20] J. R. van der Meer, S. Belkin. Where microbiology meets microengineering: Design and applications of reporter bacteria. *Nat. Rev. Microbiol.*, 2010, **8**, 511-522.
[21] E. Delatour, C. Pagnout, M. Zaffino, J. F. L. Duval. Exploiting catabolite repression and stringent response to control delay and multimodality of bioluminescence signal by metal whole-cell biosensors: interplay between metal bioavailability and nutritional medium conditions. *Biosensors,* 2022, **12**, 327.
[22] J. F. L. Duval, C. Pagnout. Decoding the time-dependent response of bioluminescent metal-detecting whole-cell bacterial sensors. *ACS Sensors*, 2019, **4**, 1373-1383.
[23] J. F. L. Duval, C. Pagnout. Bimodal stringence-mediated response of metal-detecting luminescent whole cell bioreporters: experimental evidence and quantitative theory. *Sens. Actuators B: Chemical*, 2020, **309**, 127751.
[24] R. Tecon, J. van der Meer. Bacterial biosensors for measuring availability of environmental pollutants. *Sensors,* 2008, **8**, 4062-4080.

[25] B. Li, X. Zhang, B. Tefsen, M. Wells. From speciation to toxicity: Using a "Two-in-One" whole-cell bioreporter approach to assess harmful effects of Cd and Pb. *Water Res.*, 2022, **217**, 118384.
[26] Y. Zhu, E. Elcin, M. Jiang, B. Li, H. Wang, X. Zhang, Z. Wang. Use of whole-cell bioreporters to assess bioavailability of contaminants in aquatic systems. *Front. Chem.,* 2022, **10**, 1018124
[27] M. Eigen, R. G. Wilkins. Mechanisms of Inorganic Reactions. In: Advances in Chemistry Series. Nr. 49, 1965, S. 55. American Chemical Society, Washington, D. C.
[28] R. M. Fuoss. Ionic Association. III. The Equilibrium between Ion Pairs and Free Ions. *J. Am. Chem. Soc.,* 1958, **80**, 5059-5061.
[29] M. Eigen. Uber die Kinetik sehr Schnell Verlaufender Ionenreaktionen in Wasseriger Losung. *Z. Phys. Chem.* (Frankfurt am Main) 1954, **1**, 176.
[30] R. Hajdu, J. P. Pinheiro, J. Galceran, V. Slaveykova. Modeling of Cd Uptake and Efflux Kinetics in Metal-Resistant Bacterium *Cupriavidus metallidurans*. *Environ. Sci. Technol.,* 2010, **44**, 12, 4597-4602.
[31] D. H. Nies. Efflux-mediated heavy metal resistance in prokaryotes. *FEMS Microbiol. Rev.* 2003, **27**, 313-339.
[32] N. Mirimanoff, K. J. Wilkinson. Regulation of Zn accumulation by a freshwater gram-positive bacterium (*Rhodococcus opacus*). *Environ. Sci. Technol.*, 2000, **34**, 616-622.
[33] H. P. van Leeuwen, J. Buffle, J. F. L. Duval, R. M. Town. Understanding the extraordinary ionic reactivity of aqueous nanoparticles. *Langmuir,* 2013, **29**, 10297-10302.
[34] J. F. L. Duval. Chemodynamics of metal ion complexation by charged nanoparticles: a dimensionless rationale for soft, core-shell and hard particle types. *Phys. Chem. Chem. Phys.*, 2017, **19**, 11802-11815.
[35] R. M. Town, J. F. L. Duval, J. Buffle, H. P. van Leeuwen. Chemodynamics of metal complexation by natural soft colloids: Cu(II) binding by humic acid. *J. Phys. Chem. A*, 2012, **116**, 6489-6496.
[36] J. Galceran, J. Puy, J. Salvador, J. Cecilia, H. P. van Leeuwen. Voltammetric lability of metal complexes at spherical microelectrodes with various radii. *J. Electroanal. Chem.*, 2001, **505**, 85-94.
[37] Z. Zhang, D. Alemani, J. Buffle, R.M. Town, K.J. Wilkinson. Metal flux through consuming interfaces in ligand mixtures: boundary conditions do not influence lability and relative contributions of metal species. *Phys. Chem. Chem. Phys.*, 2011, **13**, 17606-17614.
[38] L. Michaelis, M.L. Menten. Die Kinetik der Invertinwirkung. *Biochem Z.*, 1913, **49**, 333-369.
[39] T. N. P. Bosma, P. J. M. Middeldorp, G. Schraa, A. J. B. Zhender. Mass transfer limitation of biotransformation: quantifying bioavailability. *Environ. Sci. Technol.,* 1997, **31**, 248-252.
[40] J. Membrez, P.P. Infelta, A. Renken. Use of the Laplace transform technique for simple kinetic parameters evaluation. Application to the adsorption of a protein on porous beads. *Chem. Engin. Sci.,* 1996, **51**, 4489-4498.
[41] D. Delle Side, V. Nassisi, C. Pennetta, P. Alifano, M. Di Salvo., A. Talà, A. Chechkin, F. Seno, A. Trovato. Bacterial bioluminescence onset and quenching: a dynamical model for a quorum sensing-mediated property. *R. Soc. Open Sci.* 2017, **4**, 171586.
[42] C. Pagnout, R. M. Présent, P. Billard, E. Rotureau, J. F. L. Duval. What do luminescent bacterial metal-sensors probe? Insights from confrontation between experiments and flux-based theory. *Sens. Actuators B: Chemical*, 2018, **270**, 482-491.
[43] G. Yang, Q.-G. Tan, L. Zhu, K. J. Wilkinson. The role of complexation and competition in the biouptake of europium by a unicellular alga. *Environ. Toxicol. Chem.,* 2014, **33**, 2609-2615.
[44] B. A. Eijkelkamp, J. R. Morey, M. P. Ween, Ong C-lY, A. G. McEwan, J. C. Paton, C. A. McDevitt. Extracellular zinc competitively inhibits manganese uptake and compromises oxidative stress management in *Streptococcus pneumoniae*. *PLoS ONE,* 2014, **9**, e89427.

SUPPLEMENTARY INFORMATION

Kinetics of metal detection by luminescence-based whole-cell biosensors: connecting biosensor response to metal bioavailability, speciation and cell metabolism.

Jérôme F.L. Duval,[1,*] Lorenzo Maffei,[2] Eva Delatour,[2] Marie Zaffino,[2] Christophe Pagnout[2]

[1] Université de Lorraine, CNRS, LIEC, F-54000 Nancy, France.
[2] Université de Lorraine, CNRS, LIEC, F-57000 Metz, France.
* Corresponding author (jerome.duval@univ-lorraine.fr).

This document contains 5 supplementary equations and 2 supplementary figures.

I. Supplementary equations.

The complete expression of $f_{\mathrm{a,M}}$ involved in Eqs. (17) and (19) that define the time constant τ_{o} and the scalar λ_{o}, respectively, reads after algebraic arrangements as

$$f_{\mathrm{a,M}}=\frac{3\varphi}{1-\varphi}\frac{\overline{h}_{\mathrm{a}}^{-2}\dfrac{\overline{K}_{\mathrm{ML}}}{1+\overline{K}_{\mathrm{ML}}}(1-\varepsilon)\left[\overline{h}_{\mathrm{a}}\left(\varphi^{-1/3}\operatorname{sech}(\sigma)-1\right)+\tanh(\sigma)\right]+\dfrac{1}{6}\left(1-\varphi^{-1/3}\right)^{2}\left(1+2\varphi^{1/3}\right)\left(\overline{h}_{\mathrm{a}}-\tanh(\sigma)\right)}{\overline{h}_{\mathrm{a}}\left(1-\varphi^{1/3}\right)-\left(1-\varphi^{1/3}+\varepsilon\overline{K}_{\mathrm{ML}}\right)\tanh(\sigma)} \tag{S1}$$

where σ is given by $\sigma=\overline{h}_{\mathrm{a}}\left(1-\varphi^{-1/3}\right)$ and $\overline{h}_{\mathrm{a}}$ is provided by Eq. (4) in the main text. It is verified that Eq. (S1) in the limit $\varphi<<1$ reduces to Eq. (21) written in terms of the ML lability parameter ξ (Eq. (6)).

Given the expression defining $c_{\mathrm{M}}^{*}(t)$ (Eq. (14) in the main text) obtained after arrangements and Laplace transform of Eqs. (9)-(13), the dependence of the intracellular concentration of free M at *t*, $\phi_{\mathrm{M}}(t)$, can be evaluated, and the result after algebraic manipulations reads as

$$\phi_{\mathrm{M}}(t)=\frac{K_{\mathrm{H}}k_{\mathrm{int}}\tau_{\mathrm{a,i}}c_{\mathrm{M}}^{*,0}}{1+\left(p_{\mathrm{ML}}Bn\right)^{-1}}\left[\frac{\mathrm{e}^{-\frac{1+\overline{K}_{\mathrm{i}}}{\overline{K}_{\mathrm{i}}}\overline{t}}}{\overline{\omega}_{-}-\overline{\omega}_{+}}\sum_{n\equiv+,-}\delta_{n}\left(1-\frac{1}{\overline{\omega}_{n}\overline{K}_{\mathrm{i}}}\right)\left(\mathrm{e}^{\left(\frac{1+\overline{K}_{\mathrm{i}}}{\overline{K}_{\mathrm{i}}}-\overline{\omega}_{n}\right)\overline{t}}-1\right)+\frac{\overline{\tau}_{\mathrm{o}}}{\zeta+\overline{K}_{\mathrm{i}}}\left(1-\mathrm{e}^{-\frac{1+\overline{K}_{\mathrm{i}}}{\overline{K}_{\mathrm{i}}}\overline{t}}\right)\right] \tag{S2}$$

where $\delta_{n}=1$ for $n\equiv+$ and $\delta_{n}=-1$ for $n\equiv-$, and Bn, $\overline{\tau}_{\mathrm{o}}=\tau_{\mathrm{o}}/\tau_{\mathrm{a,i}}$, ζ and $\overline{\omega}_{\pm}$ are given by Eqs. (20), (17), (18) and (16), respectively, and $p_{\mathrm{ML}}\approx p_{\mathrm{o}}=1+\varepsilon\overline{K}_{\mathrm{ML}}\xi$ for $\varphi<<1$ (cf. below Eq. (5)). Combining Eqs. (12) and (S2), the time-dependent concentration of intracellular $\mathrm{MP_{reg}}$ complex, $\phi_{\mathrm{c}}(t)$, can be written in the form

$$\phi_{\mathrm{c}}(t)=\overline{K}_{\mathrm{i}}\frac{K_{\mathrm{H}}k_{\mathrm{int}}\tau_{\mathrm{a,i}}c_{\mathrm{M}}^{*,0}}{1+\left(p_{\mathrm{ML}}Bn\right)^{-1}}\left[\frac{\overline{\tau}_{\mathrm{o}}}{\zeta+\overline{K}_{\mathrm{i}}}-\frac{1}{\overline{K}_{\mathrm{i}}}\frac{1}{\overline{\omega}_{-}-\overline{\omega}_{+}}\sum_{n\equiv+,-}\delta_{n}\left(\overline{\omega}_{n}\right)^{-1}\mathrm{e}^{-\overline{\omega}_{n}\overline{t}}\right] \tag{S3}$$

From Eqs. (S2) and (S3), we infer that the concentrations of intracellular M and $\mathrm{MP_{reg}}$ complexes at $t\to\infty$, denoted as $\phi_{\mathrm{M}}^{\infty}$ and $\phi_{\mathrm{c}}^{\infty}$, respectively, are interrelated by the equilibrium expression

$$\phi_{\mathrm{M}}^{\infty} = \phi_{\mathrm{c}}^{\infty} / \bar{K}_{\mathrm{i}} = \frac{K_{\mathrm{H}} k_{\mathrm{int}} \tau_{\mathrm{o}} c_{\mathrm{M}}^{*,0}}{\left[1+\left(p_{\mathrm{ML}} Bn\right)^{-1}\right]\left(\zeta + \bar{K}_{\mathrm{i}}\right)} \tag{S4}$$

Finally, solution of Eqs. (9)-(13) leads to the following expression of the M surface concentration at equilibrium, $c_{\mathrm{M}}^{\mathrm{a}}\left(t \to \infty\right) = c_{\mathrm{M}}^{a,\infty}$,

$$c_{\mathrm{M}}^{a,\infty} / c_{\mathrm{M}}^{*,0} = \frac{1}{1+\left(p_{\mathrm{ML}} Bn\right)^{-1}} \left(c_{\mathrm{M}}^{*,\infty} / c_{\mathrm{M}}^{*,0} + \frac{k_{\mathrm{e}} \tau_{\mathrm{o}} \left(p_{\mathrm{ML}} Bn\right)^{-1}}{\left[1+\left(p_{\mathrm{ML}} Bn\right)^{-1}\right]\left(\zeta + \bar{K}_{\mathrm{i}}\right)} \right) \tag{S5}$$

where $c_{\mathrm{M}}^{*,\infty} / c_{\mathrm{M}}^{*,0}$ is defined by Eq. (22).

II. Supplementary Figures.

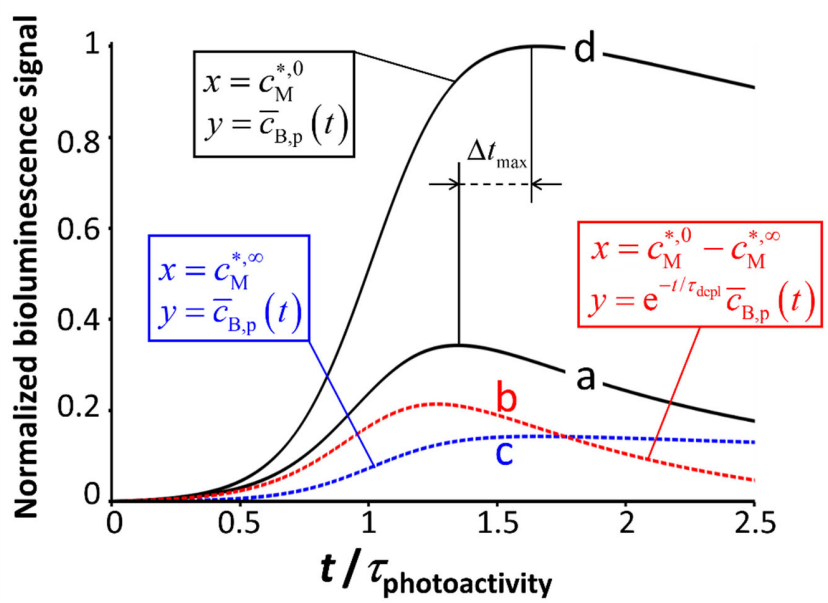

Figure S1. Illustration of the decomposition of the bioluminescence signal with account of metal depletion in bulk solution (curve (a)) on the basis of the two terms defined by Eq. (40) in the main text (curves (b) and (c)). Accordingly, the signal corresponding to curve (a) is the sum of the signals pictured by curves (b) and (c). Curve (d) represents the signal obtained without considering the effects of bulk metal depletion. All signals are here normalized by the maximum of bioluminescence reached in the absence of bulk M depletion. The time axis is scaled by $\tau_{\mathrm{photoactivity}}$ which is the time at which the (dimensionless) concentration of photoactive cells, $\bar{c}_{\mathrm{B,p}}\left(t\right)$, features an inflexion point (cf. main text for details and Figure 5A, red curve therein). The (dummy) variables *x* and *y* are those defined below Eq. (40), and they specify which bulk M concentration is applicable for computing the signals (b), (c) and (d) (variable *x*) and which expression of the concentration of photoactive cells is relevant to each signal (variable *y*). $\Delta t_{\max}$ represents the shift in position of the bioluminescence maximum as a result of bulk M depletion. Using the notations detailed in the main text (cf. Eq. (40)), curves (a), (c), (b) and (d) correspond to $\overline{Lum}\left(t\right) / \overline{Lum}_{\max}\Big|_{\varphi<<\varphi^*}$, $\overline{Lum^{(0)}}\left(t, c_{\mathrm{M}}^{*,\infty}, \bar{c}_{\mathrm{B,p}}\left(t\right)\right) / \overline{Lum}_{\max}\Big|_{\varphi<<\varphi^*}$, $\overline{Lum^{(0)}}\left(t, c_{\mathrm{M}}^{*,0} - c_{\mathrm{M}}^{*,\infty}, \mathrm{e}^{-t/\tau_{\mathrm{depl}}} \bar{c}_{\mathrm{B,p}}\left(t\right)\right) / \overline{Lum}_{\max}\Big|_{\varphi<<\varphi^*}$ and $\overline{Lum}\left(t\right)\Big|_{\varphi<<\varphi^*} / \overline{Lum}_{\max}\Big|_{\varphi<<\varphi^*}$, respectively, where

$\overline{Lum}(t) = Lum(t) / \left[c_B \left(1 - \tilde{K}_H S_a c_B \right) \right]$ and $\overline{Lum^{(0)}}(t,x,y) = Lum^{(0)}(t,x,y) / \left[c_B \left(1 - \tilde{K}_H S_a c_B \right) \right]$. Figure S1 holds for $\varphi / \varphi^* = 6$ with the model parameters adopted in Figure 5B of the main text.

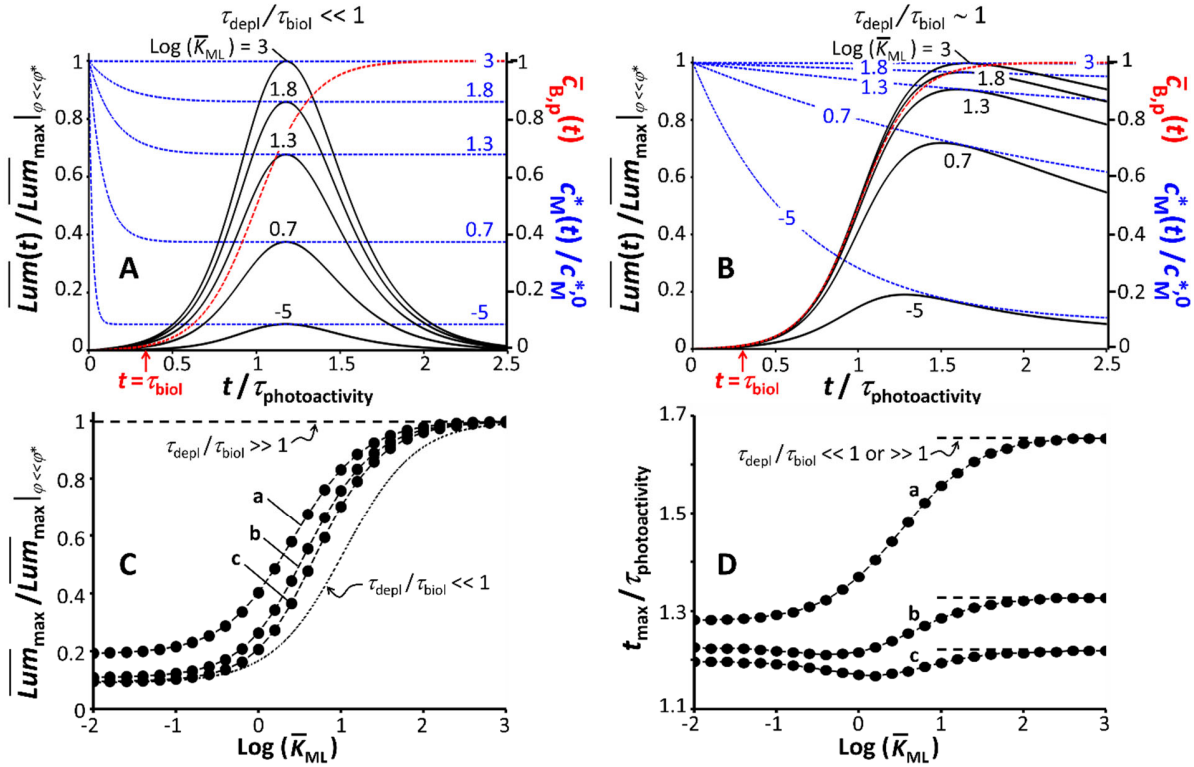

Figure S2. Illustrations of the dependence of the dimensionless bioluminescence signal $\overline{Lum}(t) / \overline{Lum}_{max}\big|_{\varphi << \varphi^*}$ (evaluated from Eq. (39)) on time for different dimensionless ML stability constants $\bar{K}_{ML}$ (indicated) for the situations $\tau_{depl} / \tau_{biol} << 1$ **(A)** and $\tau_{depl} / \tau_{biol} \sim 1$ **(B).** τ_{depl} is the timescale for depletion of bulk M concentration and τ_{biol} marks the onset of the increase in the concentration of photoactive cells $\bar{c}_{B,p}(t)$ with time (red dotted curves). The time axis is scaled by $\tau_{photoactivity}$ which is the time at which $\bar{c}_{B,p}(t)$ features an inflexion point. Blue dotted curves represent the time-dependent (dimensionless) bulk M concentration, $c_M^*(t) / c_M^{*,0}$, for each selected value of $\bar{K}_{ML}$ (Eqs. (14)-(22) or, equivalently, Eq. (25) under the conditions adopted in this figure). The (dimensionless) maxima of the bioluminescence signals and their time-positions $t_{max} / \tau_{photoactivity}$ under the conditions in **(B)** (where $\tau_{depl} / \tau_{biol} \sim 1$) are reported in **(C)** and **(D)**, respectively. We further provide in **(C)** and **(D)** the signal maxima and associated $t_{max} / \tau_{photoactivity}$, respectively, as a function of $\bar{K}_{ML}$ in the extremes $\tau_{depl} / \tau_{biol} << 1$ and $\tau_{depl} / \tau_{biol} >> 1$ for the conditions that hold in **(B)** (indicated). Unless otherwise specified in the figure, adopted model parameters are: $\varphi / \tilde{\varphi} = 10$ with $\tilde{\varphi} = \varphi^* / \left(1 + \bar{K}_{ML} \right)$ ($\tilde{\varphi}$ is independent of $\bar{K}_{ML}$), $\varepsilon = 1$, $a = 1$ μm, $D_M = 10^{-9}$ m² s^{-1}, $Bn^{-1} = 0.1$, $\xi \to 0$, $\bar{K}_i = 10$, $\tau_{a,i} = 0.1$ s, $k_r \tau_{a,i} = 10^{-4}$, $k_e = 10^{-3}$ s^{-1} **(A)**, $k_e = 10^{-4.5}$ s^{-1} **(B,C,D)**, $\tau_{photoactivity} = 15$ h in **(A)**, **(B)**, **(C)** (curve (a)) and **(D)** (curve (a)), $\tau_{photoactivity} = 30$ h for curves (b) in **(C)** and **(D)**, $\tau_{photoactivity} = 45$ h for curves (c) in **(C)** and **(D)**. The expression adopted for $F(t)$ in Eq. (39) correspond to Eq. (16) in Ref. [22]. In **(C)** and **(D)**, dotted lines connecting symbols are guides to the eye.